SARS-CoV-2 invades cognitive centers of the brain and induces Alzheimer's-like neuropathology

Wei-Bin Shen[1#], James Logue[2#], Penghua Yang[1#], Lauren Baracco[2], Montasir Elahi[1], E. Albert Reece[1, 3], Bingbing Wang[1], Ling Li[4], Thomas G Blanchard[4], Zhe Han[5], Matthew B Frieman[2], Robert A Rissman[6, 7], Peixin Yang[1, 3 *]

[1]Department of Obstetrics, Gynecology & Reproductive Sciences, University of Maryland School of Medicine, Baltimore, Maryland, USA.
[2] Department of Microbiology and Immunology, University of Maryland School of Medicine, Baltimore, MD 21201, USA.
[3]Department of Biochemistry & Molecular Biology, University of Maryland School of Medicine, Baltimore, Maryland, USA.
[4]Department of Pediatrics, University of Maryland School of Medicine, Baltimore, MD, USA.
[5]Department of Medicine, University of Maryland School of Medicine, Baltimore, MD, USA.
[6]Department of Neurosciences, University of California San Diego, La Jolla, CA, 92093.
[7]Shiley-Marcos Alzheimer's Disease Research Center, University of California San Diego, La Jolla, California, 92093.
[#] These authors contribute equally to this work.
*Correspondence: Peixin Yang, PhD, Department of Obstetrics, Gynecology & Reproductive Sciences, University of Maryland School of Medicine, BRB11-039, 655 W. Baltimore Street, Baltimore, MD, 21201. Email: pyang@som.umaryland.edu, Tel: 410-706-8402, Fax: 410-706-5747.

Conflict of interest statement: The authors have declared that no conflict of interest exists
Subheading: Neurodegenerative phenotypes in COVID-19

Keywords: SARS-CoV-2; neurons; iPSC; Alzheimer's; COVID-19 brains; Alzheimer's infectious etiology; beta-amyloid; neuroinflammation; tauopathy.

Abstract

Major cell entry factors of SARS-CoV-2 are present in neurons; however, the neurotropism of SARS-CoV-2 and the phenotypes of infected neurons are still unclear. Acute neurological disorders occur in many patients, and one-third of COVID-19 survivors suffer from "brain diseases". Here, we show that SARS-CoV-2 invades the brains of five patients with COVID-19 and Alzheimer's, autism, frontotemporal dementia or no underlying condition by infecting neurons and other cells in the cortex. SARS-CoV-2 induces or enhances Alzheimer's-like neuropathology with manifestations of β-amyloid aggregation and plaque formation, tauopathy, neuroinflammation and cell death. SARS-CoV-2 infects mature but not immature neurons derived from inducible pluripotent stem cells from healthy and Alzheimer's individuals through its receptor ACE2 and facilitator neuropilin-1. SARS-CoV-2 triggers Alzheimer's-like gene programs in healthy neurons and exacerbates Alzheimer's neuropathology. A gene signature defined as an Alzheimer's infectious etiology is identified through SARS-CoV-2 infection, and silencing the top three downregulated genes in human primary neurons recapitulates the neurodegenerative phenotypes of SARS-CoV-2. Thus, SARS-CoV-2 invades the brain and activates an Alzheimer's-like program.

Introduction

The COVID-19 pandemic caused by severe acute respiratory syndrome coronavirus 2 (SARS-CoV-2) has infected at least 213 million people worldwide and 37.8 million Americans to date. SARS-CoV-2 not only causes respiratory syndromes but also leads to neurological abnormalities, with an 85% occurrence rate in patients with Alzheimer's disease [1,2]. In fact, neurological symptoms, including hypogeusia, headache and anosmia, precede the onset of respiratory symptoms in the majority of patients with COVID-19. The major chronic sequelae of COVID-19 are expected to be cognitive decline and dementia [3]. A recent study has shown that one-third of COVID-19 survivors exhibit substantial neurological and psychiatric morbidity in the 6 months after SARS-CoV-2 infection [4]. Furthermore, the "brain disease" risk is not limited to patients who have severe COVID-19 [4]. Thus, the COVID-19 pandemic provides a unique but unwelcomed opportunity to study the contribution of SARS-CoV-2 to neurological disorders, including Alzheimer's disease.

It has been proposed that β-coronaviruses, including SARS-CoV-2, can invade the central nervous system [5]. The two coronaviruses closely related to SARS-CoV-2, Middle Eastern respiratory syndrome coronavirus (MERS-CoV) and severe acute respiratory syndrome coronavirus 1 (SARS-CoV-1), can infect the central nervous system [6,7]. A recent study showed the presence of SARS-CoV-2 in a patient's olfactory mucosa and its neuronal projections [8]. In addition to olfactory transmucosal entry of SARS-CoV-2 into the central nervous system (CNS) [8], other potential routes of SARS-CoV-2 brain entry, including blood–brain barrier (BBB) passage, especially under conditions of a compromised BBB, such as in cases of Alzheimer's disease and autism [9,10], and the infiltration of infected immune cells have been proposed [11], though evidence for infected immune cells remains scarce. However, neurological disorders are not limited to severe COVID-19 cases, suggesting that multiple brain entries may account for SARS-CoV-2 neurotropism. Although SARS-CoV-2 can enter the brain, experimental evidence of its presence in key

brain regions involved in cognitive functions is still lacking, and little is known about the functional impact of SARS-CoV-2 CNS invasion on neurons.

SARS-CoV-2 entry into host cells is facilitated by its cell surface receptors. The spike proteins of both SARS-CoV-2 and the earlier SARS-CoV-1 bind to angiotensin-converting enzyme 2 (ACE2) as the first step of cellular entry [12]. The presence of ACE2 in neurons of the brain has been demonstrated [13]. However, ACE2 is expressed at relatively low levels in most tissues [14]. SARS-CoV-2 exhibits much higher infectivity than SARS-CoV-1. This evidence implicates either the existence of other cell surface receptors in SARS-CoV-2 cell entry or the facilitation of cell entry by other factors. Indeed, neuropilin-1 (NRP1) has been identified as a facilitator of SARS-CoV-2 entry when ACE2 is expressed, leading to high rates of infection [14]. NRP1 effectively binds to the protease furin-cleaved spike protein of SARS-CoV-2 [14], a process that does not occur for SARS-CoV-1. NRP1 is abundantly expressed in cells of many tissues including neurons [15]. The presence of ACE2 and NRP1 in neurons suggests the high possibility of neurotropism. It is of interest to determine in which cell types in the CNS and at which stage of neural development SARS-CoV-2 can exert its infectibility.

There is a profound link between SARS-CoV-2 infection and dementia/Alzheimer's disease. The 2002 and 2012 SARS and MERS epidemics caused memory impairment in many recovered patients [16]. Neurological syndromes related to Alzheimer's disease, including neuroinflammatory syndromes [17,18], seizures [19], delirium [20,21], and alterations in personality, behavior, and cognitive deficits [17,22], frequently occur in patients with COVID-19 who recover from COVID-19. Thus, SARS-CoV-2 infection of the brain may increase the risk of Alzheimer's disease. The direct effects of SARS-CoV-2 on neuronal function and survival, the inflammatory cytokine response, and hypoxia may lead to an Alzheimer's-like manifestation [23,24]. Additionally, Alzheimer's patients have twice the risk of contracting COVID-19, which deteriorates Alzheimer's symptoms and increases mortality [25]. The cellular mechanism underlying the possible

93 neurotropism of SARS-CoV-2 needs to be revealed for the development of possible treatments for a large
94 number of COVID-19 survivors suffering from neurological disorders.

95 In this study, we sought to test whether SARS-CoV-2 is neurotropic and infects neural cells in the
96 cognitive center in five patients with Alzheimer's disease, autism, frontotemporal dementia and no
97 underlying condition, respectively. SARS-CoV-2 infection alters transcriptomic landscapes in favor of the
98 development of Alzheimer's-like neuropathology in non-Alzheimer's individuals and exacerbates
99 Alzheimer's neuropathology in patients with Alzheimer's. We found that SARS-CoV-2 invades the
100 cognitive centers of all five COVID-19 patients, leading to Alzheimer's-like neuropathology or
101 Alzheimer's neuropathology exacerbation. SARS-CoV-2 infects human inducible pluripotent stem cell
102 (iPSC)-derived mature neurons from healthy individuals, leading to amyloid beta (Aβ) deposition,
103 increased inflammation, neuronal death and increased expression of Alzheimer's mediators. Strikingly,
104 we found that SARS-CoV-2-infects neurons from healthy individuals through a shared gene expression
105 program with Alzheimer's neurons, leading to activation of the infectious pathways and supporting the
106 infectious etiology of Alzheimer's disease.

107

Results

SARS-CoV-2 invades cognitive centers of the brain

Because ACE2, the SARS-CoV-2 cellular receptor, and NRP1, a facilitator of SARS-CoV-2 entry, are expressed in CNS neurons, we hypothesized that SARS-CoV-2 can infect neural cells in the brain, especially under conditions such as Alzheimer's disease and autism with BBB compromise. SARS-CoV-2 has been observed in cells of olfactory bulbs. We focused on cognitive centers of the brain. The SARS-CoV-2 spike protein and nucleocapsid protein were detected in cells of the inferior frontal cortexes of five COVID-19 cases: two autism cases, one Alzheimer's case, one frontotemporal dementia (FTD) case and one case without any underlying health conditions (apparently healthy case) (Fig. 1, Fig. S1). In contrast, there was no positive staining of spike protein or nucleocapsid protein in the cortexes of the non-COVID-19 autism brains (Fig. 1A, C, Fig. S1A). Spike protein- and nucleocapsid protein-positive viral particles were robustly present in the cytoplasm and cellular projections of cortical cells (Fig. 1E, F). RNAscope *in situ* hybridization detected the abundant presence of SARS-CoV-2 genomic RNA in cortical cells of the five COVID-19 cases (Fig. 1G, H; Fig. S1F). PCR analysis using the CDC method [26] confirmed the presence of SARS-CoV-2 RNA in the three cases that had frozen brain tissues (Fig. 1I). In the 31-year-old COVID-19 autism case, the amounts of SARS-CoV-2 RNA in the inferior frontal cortex and the dorsolateral prefrontal cortex were comparable to those in the lungs (Fig. 1I). In the COVID-19 FTD case and the COVID-19 apparently healthy case, SARS-CoV-2 RNA was also detected, whereas there was no SARS-CoV-2 RNA in the age-matched non-COVID-19 FTD individual or in the age-matched non-COVID-19 apparently healthy individual (Fig. 1I).

Additional analyses showed that cells of the three cortical regions, the entorhinal cortex, the inferior frontal cortex and the dorsolateral prefrontal cortex, in the two COVID-19 autism cases and the COVID-19 Alzheimer's case possessed abundant spike protein staining signals (Fig. 1J, K, L). The

131 numbers of SARS-CoV-2 spike protein-positive cells in these three regions were different in these three
132 COVID-19 cases (Fig. 1J, K, L). These findings demonstrated that SARS-CoV-2 was neurotropic in this
133 cohort of COVID-19 patients (Table S1).

134 **SARS-CoV-2 infects CNS cells expressing ACE2 and NRP1**

135 Because SARS-CoV-2 exists in cortical cells in COVID-19 patients, these cells must express ACE2
136 and NRP1. Indeed, the SARS-CoV-2 spike protein staining signal was colocalized with both ACE2 and
137 NRP1 signals (Fig. 2A, B), indicating that SARS-CoV-2 infects cortical cells using these proteins. ACE2
138 was colocalized with the neuron marker neurofilament light chain (NFL) (Fig. 2C, D), the pan-neuron
139 marker class III beta-tubulin (Tuj1) (Fig. 2E), the oligodendrocyte marker 2',3'-cyclic nucleotide-3'-
140 phosphodiesterase (CNPase) (Fig. 2F), and the microglia marker ionized calcium-binding adapter
141 molecule 1 (Iba1) (Fig. 2G). Quantitative analysis of double ACE2 and cell marker positive cells indicated
142 that all neurons expressed ACE2 (Fig. 2H). Next, we determined which cell types in the cortexes were
143 infected by SARS-CoV-2. We used dual immunohistological labeling with antibodies against cell type-
144 specific markers and the SARS-CoV-2 spike protein. Both the mature neuron marker neuronal nuclear
145 protein (NeuN) and the pan-neuron marker class III beta-tubulin (Tuj1) were colocalized with the spike
146 protein in cells of the inferior frontal cortex (Fig. 2I, J). In the same region, both GABAergic inhibitory
147 neurons (GAD65-positive) and glutamatergic excitatory neurons (glutamine synthetase-positive)
148 contained SARS-CoV-2 spike protein staining signals (Fig. 2K, L). The SARS-CoV-2 spike protein
149 staining signal was also present in Iba1-positive microglia and CNPase-positive oligodendrocytes in the
150 same region (Fig. 2M, N). However, there was no detectable SARS-CoV-2 spike protein staining signal
151 in glial fibrillary acidic protein (GFAP)-positive astrocytes (Fig. 2O). Quantification of double SARS-
152 CoV-2 spike protein- and different cell type marker-positive cells indicated that spike protein was present
153 in all neurons (Fig. 2P). Thus, SARS-CoV-2 infects various CNS cell types. Because infected peripheral

154 immune cells may enter the brain, T and B cells were examined in the inferior frontal cortex. There were
155 no T, B cell, or macrophage marker staining signals in this region of the COVID-19 autism cases (Fig.
156 S2). However, a significant number of these immune cells were detected in the COVID-19 Alzheimer's
157 brain (Fig. S2).

158 **SARS-CoV-2 causes cell death via multiple pathways**

159 To determine whether SARS-CoV-2-infected cells in the cortical regions undergo cell death, we used
160 immunohistological dual labeling with antibodies against the spike protein and cleaved caspase-3. There
161 was no detectable cleaved caspase 3 staining signal in cells of the inferior frontal cortexes of non-COVID-
162 19 autism controls (Fig. 3A). Over 90% of cleaved caspase 3-positive cells were SARS-CoV-2 spike
163 protein positive in the cortexes of two COVID-19 autism cases (Fig. 3A). In the COVID-19 Alzheimer's
164 disease case, over 20% of cleaved caspase 3-positive cells were SARS-CoV-2 spike protein positive (Fig.
165 3B). Cleaved caspase 3 was induced in two COVID-19 autism cases and the COVID-19 case without
166 underlying health conditions and was enhanced in the COVID-19 Alzheimer's case and the COVID-19
167 FTD case (Fig. S3A, B, C).

168 To further determine the type of programmed cell death, we examined the presence of necroptotic,
169 ferroptotic, and senescent cells. The cell necroptosis markers phospho-MLKL (mixed lineage kinase
170 domain-like) and phospho-RIPK3 coexisted in spike protein-positive cells (Fig. 3C, Fig. S3D). Similarly,
171 the two cell ferroptosis markers TfR1 (transferrin receptor) and ASCL4 (long-chain fatty acyl-CoA
172 synthetase 4) were expressed in cells with positive spike protein signals (Fig. 3D, Fig. S3E). Because the
173 cytokine associated with SARS-CoV-2 may trigger the cellular senescence program, we detected the
174 senescence marker DPP4 (dipeptidyl-peptidase 4) in a subset of spike protein-positive cells (Fig. 3E).
175 There were negligible double spike protein- and TfR1- or p-RIPK3-positive cells in the COVID-19
176 Alzheimer's case (Fig. 3D, Fig. S3D). These findings suggest that SARS-CoV-2 leads to cell death and

177 senescence through multiple pathways.

178 **SARS-CoV-2 induces neuroinflammation**

179 It has been suggested that SARS-CoV-2 infection leads to neuroinflammation. However, direct
180 evidence on the link between SARS-CoV-2 and neuroinflammation is still lacking. The protein expression
181 of two cytokines, IL-1β and IL-6 (interleukin 6), was significantly increased in the cortical cells of
182 COVID-19 autism patients compared to the cortical cells of non-COVID-19 autism patients (Fig. S4A, B,
183 C), providing the direct evidence of neuroinflammation induced by SARS-CoV-2.

184 **SARS-CoV-2 induces Alzheimer's-like phenotype development and exacerbation**

185 Cellular Aβ (amyloid beta) aggregates were observed in the cortexes of the two COVID-19 autism
186 cases (Fig. 4A) and the one COVID-19 case without underlying health conditions (Fig. 4B), whereas it
187 was not present in the cortexes of age-matched non-COVID-19 autism cases and an apparently healthy
188 individual (Fig. 4A, B). Extracellular Aβ plaques were present in one of the COVID-19 autism cases (Fig.
189 4A). Immunofluorescence analysis with thioflavin-T confirmed that the cytoplasmic deposition of Aβ in
190 the COVID-19 autism cases consisted of aggregated Aβ (Fig. 4A). There was more Aβ plaque deposition
191 per measured area in the cortexes of the COVID-19 Alzheimer's and FTD brains than in the cortexes of
192 age-matched non-COVID-19 Alzheimer's and FTD brains (Fig. 4C, D). One of the neuropathological
193 hallmarks of Alzheimer's disease is the development of intracellular neurofibrillary tangles (NFTs)
194 composed of hyperphosphorylated Tau (microtubule-associated protein tau). p-Tau-containing NFTs are
195 associated with neuronal dysfunction, cognitive deficits and neuronal death [27,28]. p-Tau-containing NFTs
196 were present in the inferior cortexes of the two COVID-19 autism cases (Fig. 4E). Cellular p-Tau
197 deposition was induced in these two COVID-19 autism cases and the COVID-19 case without underlying
198 health conditions (Fig. 4E, F), whereas there were no signals or negligible p-Tau staining signals in the
199 cortexes of non-COVID-19 control brains (Fig. 4E, F). There were significantly higher numbers of Pick

200 bodies in the COVID-19 FTD case than in age-matched non-COVID-19 FTD cases (Fig. 4G, H). Thus,
201 SARS-CoV-2 infection is linked to Alzheimer's neuropathology.

202 **SARS-CoV-2 infects iPSC-derived mature neurons**

203 Based on the above findings in neurons of COVID-19 patients' brain cortexes, we propose that SARS-
204 CoV-2 can effectively infect neurons. To establish an *in vitro* platform to study this process, we obtained
205 iPSCs derived from age-matched healthy individuals and Alzheimer's patients and differentiated it into
206 neurons, followed by SARS-CoV-2 infection. SARS-CoV-2-GFP (in which GFP replaced the viral open
207 reading frame ORF7a [29]) at a multiplicity of infection (MOI) of 0.1 or 0.2 did not infect any cells at iPSC
208 neuron differentiation day 35 (Fig. 5A, Fig. S5A) and some of these cells expressed the pan-neuron marker
209 Tuj1 but did not express the mature neuron marker NeuN (Fig. 5B, Fig. S5B). At iPSC differentiation day
210 50, SARS-CoV-2-GFP at an MOI of 0.05, 0.1 or 0.2 effectively infected cells differentiated from iPSCs
211 from healthy individuals and Alzheimer's patients (Fig. 5C, Fig. S5C, D), and SARS-CoV-2-GFP could
212 be detected in cell culture media 72 hours post SARS-CoV-2-GFP infection (Fig. 5D), indicating that the
213 virus not only infects cells but also replicates intracellularly. SARS-CoV-2-infected cells were essentially
214 all Tuj1-positive cells at iPSC differentiation day 50 (Fig. 5E), and no GFAT-positive astrocytes were
215 detected in mock- and SARS-CoV-2-infected cells (Fig. 5F). At iPSC differentiation day 35, there was no
216 expression of ACE2 or NRP1 proteins (Fig. 5G, H). At iPSC differentiation day 50, robust ACE2 and
217 NRP1 protein expression existed in Tuj1-positive neurons (Fig. 5I, J). Over 40% of Tuj1-positive neurons
218 were ACE2- and/or NRP1-positive (Fig. 5I, J). Subsequent experiments were conducted on iPSC
219 differentiation day 50. These results suggest that SARS-CoV-2 infects mature neurons via ACE2 with the
220 facilitation of NRP1.

221 **SARS-CoV-2 induces Alzheimer's phenotypes in iPSC-derived cells**

222 Because SARS-CoV-2 induces Aβ cellular aggregates and extracellular plaques, p-Tau cellular

223 deposition and NFTs and neuroinflammation in COVID-19 patients, we hypothesized that SARS-CoV-2
224 infection can turn neurons derived from iPSCs from healthy individuals into Alzheimer's-phenotype
225 neurons. Neurons differentiated from iPSCs of healthy individuals and Alzheimer's patients were infected
226 with wild-type SARS-CoV-2 (WA-1 strain [30]) at an MOI of 0.1 for 48 hours (Fig. 6, Fig. S6). SARS-CoV-
227 2 induced cellular Aβ aggregates in healthy neurons and increased cellular Aβ aggregates in Alzheimer's
228 neurons (Fig. 6A). Cellular p-Tau deposition was induced in healthy neurons after 72 hours of SARS-
229 CoV-2 infection (Fig. 6B), and the virus further increased cellular p-Tau deposition in Alzheimer's neurons
230 (Fig. 6B). Compared to their mock-infected counterparts, both healthy neurons and Alzheimer's neurons
231 had higher levels of major inflammatory cytokines including IL-1β, IL-6, IFNγ and TNFα after SARS-
232 CoV-2 infection (Fig. 6C). Among the critical Alzheimer's mediators, amyloid precursor protein (APP),
233 enzyme β-secretase 1 (BACE1), and presenilin 1/2 (PSEN1/2), SARS-CoV-2 significantly increased
234 BACE1 expression in healthy neurons and Alzheimer's neurons but did not affect the expression of the
235 other Alzheimer's mediators (Fig. 6D, E). Likewise, SARS-CoV-2 significantly increased the number of
236 cleaved caspase 3-positive cells differentiated from iPSCs of healthy individuals and Alzheimer's patients
237 (Fig. 6F). Thus, SARS-CoV-2 triggers an Alzheimer's-like cellular program in neurons derived from
238 iPSCs of healthy individuals and enhances Alzheimer's phenotypes in cells derived from Alzheimer's
239 iPSCs.

240 **Alzheimer's infectious etiology genes identified via SARS-CoV-2**

241 Over 95% of Alzheimer's cases are sporadic and their causes are still unclear. Studies of DNA viruses
242 have shown that Alzheimer's etiology has an infectious component [31,32]. Based on the above observation
243 that SARS-CoV-2 induces Alzheimer's phenotypes in neurons derived from iPSCs of healthy non-
244 Alzheimer's individuals, we aimed to utilize SARS-CoV-2 infection to reveal genes responsible for the
245 Alzheimer's infectious etiology. The transcriptomes of neurons differentiated from iPSCs of healthy

individuals and Alzheimer's patients were determined by RNA sequencing (Fig. 7A-E). Under mock infection conditions, 553 genes were significantly upregulated, while 71 genes were significantly downregulated, in Alzheimer's neurons compared to neurons from iPSCs of healthy individuals (designated healthy neurons) (Fig. 7A). SARS-CoV-2 upregulated 75 genes and downregulated 19 genes in healthy neurons (Fig. 7B). To extract the genes responsible for Alzheimer's infectious etiology, 24 overlapping genes were identified between the Alzheimer's neuron-mock-infected group and the healthy neuron-SARS-CoV-2-infected group (Fig. 7D). Pathway analysis revealed that the changes in these 24 genes activated infection pathways elicited by bacteria and viruses (Fig. 7D).

Compared to healthy neurons without viral infection, Alzheimer's neurons infected with SARS-CoV-2 had 517 upregulated genes and 256 downregulated genes (Fig. 7C). This number of downregulated genes (256) was higher than the number of downregulated genes in Alzheimer's neurons (71) (Fig. 7A, C). In Alzheimer's neurons, SARS-CoV-2 further increased the expression of 25 upregulated genes and decreased the expression of 34 downregulated genes by several-fold (Fig. S6A), indicating that the virus deteriorates Alzheimer's conditions, and pathway analysis pointed to the further activation of neuroinflammation and other processes in Alzheimer's neurons (Fig. S6B).

Top genes in the Alzheimer's infectious etiology transform neurons

The 24 overlapping genes between Alzheimer's neurons without SARS-CoV-2 infection and healthy neurons infected by SARS-CoV-2 are potential genes involved in the Alzheimer's infectious etiology. To evaluate whether the top upregulated genes among these 24 genes can turn healthy neurons into Alzheimer's-like neurons, we overexpressed the top three genes individually, FCGR3, LILRB5 and OTOR, in human primary neurons from a heathy individual. Overexpression of these genes in healthy neurons did not trigger cellular Aβ aggregation or cellular p-Tau deposition (Fig. S7D). In contrast, when the top three downregulated genes in the 24-gene list, GJA8, CryAA2 and PSG6, were individually

269 silenced in healthy human neurons, cellular expression of Aβ42 and p-Tau, cellular Aβ aggregation and
270 cellular p-Tau deposition were induced (Fig. 7F, Fig. S7E). Furthermore, silencing these top three
271 downregulated genes simultaneously in healthy human neurons robustly triggered cellular Aβ aggregation
272 and cellular p-Tau deposition (Fig. 7G). Thus, silencing the top three downregulated genes reprogrammed
273 healthy human neurons into Alzheimer's-like neurons.
274

275 **Discussion**

276 Although it is still controversial whether SARS-CoV-2 invades patients' brains [33,34], we provide strong
277 evidence that SARS-CoV-2 can invade the cognitive centers of the brain, leading to Alzheimer's-like
278 phenotypes and exacerbation of Alzheimer's neuropathology. Examination revealed that iPSC-derived
279 neurons infected by SARS-CoV-2 recapitulated the key aspects related to clinically observed neurological
280 disorders in COVID-19 patients and survivors: neurotropism and Alzheimer's induction or enhancement
281 by SARS-CoV-2.

282 Our observations from both COVID-19 autism and Alzheimer's brains support the effective
283 infection of neurons, oligodendrocytes and other brain cells by SARS-CoV-2. Thus, the present study
284 demonstrates the neurotropism of SARS-CoV-2. Such neurotropism has long been known to occur for
285 other types of human respiratory coronaviruses [35]. Consistent with the current findings, in human iPSC-
286 derived brain sphere neurons, SARS-CoV-2 at a dose equivalent to that in the present study has been found
287 to not only infect neurons but also replicate itself in these neurons [36]. SARS-CoV-2 viral particles are
288 present in both neuronal cell bodies and neurites [36]. SARS-CoV-2 can effectively infect cortical-like
289 neurons in iPSC-derived brain organoids and these neurons express the SARS-CoV-2 receptor ACE2 and
290 key coronavirus entry-associated proteases [37]. Regarding the infectibility of human brains by SARS-CoV-
291 2, viral RNA has been detected in 36.4% of brain biopsies of fatal COVID-19 cases [38], suggesting that
292 SARS-CoV-2 invades some COVID-19 patients' brains but may not invade all patients' brains. The current
293 study examined cortical neurons of the brains of COVID-19 patients with either autism or Alzheimer's
294 disease and observed full infectibility by SARS-CoV-2 in all cases. Similarly, a recent study using spike
295 protein staining demonstrated that SARS-CoV-2 was present in some brain regions in all three COVID-
296 19 cases studied [33]. Using multiple approaches, we showed the presence of spike and nucleocapsid proteins
297 and SARS-CoV-2 viral particles in the cortical regions of all three COVID-19 cases with either autism or

298 Alzheimer's.

299 An early study showed no evidence of SARS-CoV-2 infection of neurons [39]. In iPSC-derived brain
300 organoids, SARS-CoV-2 infects only mature choroid plexus cells, not neurons or glial cells [39]. This
301 discrepancy may be due to the different developmental stages of neurons. We show that iPSC-derived
302 immature neurons do not express ACE2 and NPR1 and thus are not able to be infected by SARS-CoV-2,
303 whereas mature neurons do express these two SARS-CoV-2 receptors and are infected by this virus.
304 Pellegrini et al. [39] did not observe ACE2 expression in neurons. In COVID-19 patients, not all neurons are
305 infected by SARS-CoV-2 [33], suggesting that different types of neurons have differential expression of
306 ACE2 and other SARS-CoV-2 entry factors and variable SARS-CoV-2 infectability. We and others [33] have
307 shown that cortical neurons including excitatory and inhibitory neurons, are able to be infected by SARS-
308 CoV-2.

309 SARS-CoV-2 enters hosts through their noses, mouths and eyes; thus, the anatomical proximity
310 between the nasal cavity/nasopharynx and the olfactory mucosa may enable olfactory transmucosal entry
311 of SARS-CoV-2 into the CNS [8]. The other major CNS entry route may depend on BBB leakage in
312 conditions of autism and Alzheimer's disease [9,10]. This may have been the case in our study, in which three
313 COVID-19 patients had either autism or Alzheimer's disease. The BBB entry route is supported by a direct
314 observation of BBB damage in COVID-19 patients [40]. Furthermore, the SARS-CoV-2 spike protein can
315 disrupt human BBB integrity in 3D microfluidic *in-vitro* models [41]. The infiltration of infected immune
316 cells into the brain has been proposed as a potential CNS entry route [11]. In agreement with a prior report,
317 no sign of infected immune cell infiltration into COVID-19 autism patients' brains was found in the
318 present study. Immune cells were present in the cortex in the COVID-19 Alzheimer's case. Thus, BBB
319 leakage may be the major CNS entry route for SARS-CoV-2 into autism brains.

320 Apoptotic cell death is observed in the cells of brain organoids infected with SARS-CoV-2 [33,37,42,43].

321 SARS-CoV-2-infected cells may not be very susceptible to apoptosis because the majority of cells
322 undergoing apoptosis are noninfected but adjacent to SARS-CoV-2-positive cells [33]. The causes of
323 apoptosis may be SARS-CoV-2-induced cellular inflammation and hypoxia, which occur in brain
324 organoids infected by this virus [33,42]. In COVID-19 patients, we found that apoptosis mostly occurred in
325 cells infected by SARS-CoV-2. We found that cellular inflammation was induced in both iPSC-derived
326 neurons and COVID-19 patient cortexes, suggesting that cellular inflammation is the primary factor
327 leading to cell death. Other factors such as p-Tau, as detected by our group and others [43], may also play
328 important roles in defining cell fates. SARS-CoV-2 infection induces not only apoptosis but also other
329 nonapoptotic cell death programs, such as necroptosis and ferroptosis, as well as senescence [44], as
330 observed in the current study. Thus, SARS-CoV-2 infection alters cellular programs, leading to critical
331 cell mass loss and cellular dysfunction.

332 COVID-19 patients and survivors experience Alzheimer's-like neural syndrome including
333 memory loss, delirium and cognitive deficits [22], suggesting that there is a cellular mechanism underlying
334 these phenomena. A prior study showed altered distribution of Tau from axons to soma and Tau
335 hyperphosphorylation in neurons of brain organoids exposed to SARS-CoV-2 [43]. We observed p-Tau
336 tangles in the cortexes of two young autism COVID-19 patients, suggesting that neurodegenerative
337 characteristics manifest in COVID-19 patients' brains. Aβ deposition and neuroinflammation were also
338 present in the cognitive centers of these two young autism COVID-19 patients and in iPSC-derived
339 neurons infected by SARS-CoV-2. These observations potentially explain the Alzheimer's-like brain
340 disease observed in individuals exposed to SARS-CoV-2.

341 The pathogenesis of Alzheimer's disease contains an element of infectious disease pathogenesis.
342 Pathogen infections can lead to the onset and progression of Alzheimer's disease. Insertions of viral DNA
343 genomes into spontaneous late-onset Alzheimer's patient genomes have been determined [31]. Viral DNA

344 insertions in the host genome correlate with the induction of critical Alzheimer's mediators, such as
345 enzymes involved in Aβ species production, aggregation and plaque formation [31]. Direct evidence for the
346 involvement of viral DNA in Alzheimer's pathogenesis comes from the demonstration that herpes simplex
347 virus type I (HSV-1) induces multicellular amyloid plaque–like structure formation, gliosis, and
348 neuroinflammation in iPSC-derived neural cells and a 3D human brain-like model [32]. We provide direct
349 evidence that the COVID-19 pandemic-causing virus SARS-CoV-2 triggers an Alzheimer's-like
350 molecular program involving a group of 24 genes related to infectious disease pathway activation. The β-
351 secretase BACE1, which produces all monomeric forms of amyloid-β (Aβ), including Aβ42, was induced
352 by SARS-CoV-2 in iPSC-derived neurons from healthy individuals; thus, BACE1 may be a primary driver
353 of the Alzheimer's-like phenotypes induced by SARS-CoV-2. SARS-CoV-2-induced hypoxia [33] may be
354 responsible for BACE1 induction because hypoxia facilitates Alzheimer's pathogenesis by inducing
355 BACE1 expression [45]. Because 26 of the 29 SARS-CoV-2 proteins physically associate with many proteins
356 in human cells [46], it is also possible that one or some of the 29 SARS-CoV-2 proteins interact with
357 transcriptional regulators in host cells, leading to BACE1 upregulation. The mechanism underlying
358 SARS-CoV-2-induced Alzheimer's-like phenotypes needs to be further investigated.

359 In summary, we found that SARS-CoV-2 neurotropism exhibited full penetrance in the cortexes
360 of COVID-19 autism and Alzheimer's patients. SARS-CoV-2 infection induced Alzheimer's-like
361 phenotypes in autism patients and exacerbated neuropathology in Alzheimer's patients. SARS-CoV-2
362 infection triggered cellular and molecular Alzheimer's pathogenesis programs in iPSC-derived neurons
363 from healthy individuals and enhanced neuropathological phenotypes in iPSC-derived neurons from
364 Alzheimer's patients. We reveal a list of 24 genes that potentially mediate the infectious etiology of
365 Alzheimer's disease under the condition of SARS-CoV-2 infection.
366

Acknowledgments

This work was supported by NIH grants R01HD100195, R01HD102206, R01HD099843, R01DK083243, R01DK101972, R01HL131737, R01HL134368, R01HL139060, R01DK103024 and P30-AG062429. No potential conflicts of interest relevant to this article are reported. The authors thank Jeffrey Metcalf, Sara Shuldberg and Sophia Perrott from the Rissman lab and UCSD Shiley-Marcos ADRC for technical assistance with this project.

Author Contributions

Shen WB, Penghua Yang, Montasir M, Xu C, Logue J, and Baracco L researched the data. Frieman M, Reece EA, Blanchard T, Li L, Han Z, and Rissman R analyzed the data and revised the manuscript. Peixin Yang conceived the project, designed the experiments, and wrote the manuscript. All authors approved the final version of the paper.

Declaration of Interests

The authors declare no competing interests.

383 **Main figure titles and legends**

384 **Figure 1. SARS-CoV-2 is present in cortical cells in COVID-19 patients.**

385 Representative images of SARS-CoV-2 spike protein staining in the inferior frontal cortexes of an age-
386 matched non-COVID-19 autism (ASD) case (**A**) and a COVID-19 autism case (ID #6437) (**B**).
387 Representative images of SARS-CoV-2 nucleocapsid protein in the inferior frontal cortexes of an age-
388 matched non-COVID-19 autism case (**C**) and a COVID-19 autism case (ID #6437) (**D**).
389 High-magnification imaging indicated that spike protein-positive (**E**) or nucleocapsid protein-positive (**F**)
390 viral particles were located in both the cytoplasm and cellular processes (arrows).
391 SARS-CoV-2 genomic RNA was detected by RNAscope in the cortical cells of the COVID-19 autism
392 case (**H,** arrows) but not in the age-matched non-COVID-19 autism case (**G**).
393 COVID-19 PCR test revealed SARS-CoV-2 positivity in brain regions of two COVID-19 cases along with
394 lung positivity (ID #6436) (**I**). Red * indicates nonspecific bands compared to the 72 bp positive band.
395 Melt curve analysis and DNA sequencing of PCR products confirmed SARS-CoV-2 positivity in brain
396 tissues.
397 SARS-CoV-2 spike protein staining positivity in the EC, IFC and DPC in the COVID-19 Alzheimer's case
398 (ID #6435) (**J**) and in COVID-19 autism case 1 (ID #6436) (**K**) and case 2 (ID #6437) (**L**). The spike
399 protein-positive cells per mm^2 were quantified in the three brain regions. Cells were counted from at least
400 3 sections ($n \geq 3$). EC: Entorhinal cortex; IFC: inferior frontal cortex; DPC: dorsolateral prefrontal cortex.
401 Scale bars: A-D, J-L = 20 μm; E, F = 10 μm; G, H = 5μm. * indicate significant difference ($P < 0.05$) by
402 one-way ANOVA and *Tukey* test.

403 **Figure 2. hACE2-positive or neuropilin 1 (NRP1)-positive neurons and nonneuronal cells exhibit**
404 **SARS-CoV-2 positivity.**

405 (**A**) Double spike protein (SP, Ni-DAB: black signals)- and hACE2 (AP staining: red signals)-positive

406 cells in the inferior frontal cortexes (IFCs) of the COVID-19 autism cases, the COVID-19 Alzheimer's
407 case and their age-matched control cases: non-COVID-19 autism control cases and non-COVID-19
408 Alzheimer's cases. The graphs show the percentages of double positive cells among total hACE2 positive
409 cells in n $\geq$ 5 random fields.
410 (**B**) Double SP (Ni-DAB: black signals)- and NRP1 (AP staining: red signals)-positive cells in the inferior
411 frontal cortexes of the COVID-19 autism cases, the COVID-19 Alzheimer's case and their age-matched
412 control cases. The graphs show the percentages of double positive cells among total NRP1-positive cells
413 in n $\geq$ 5 random fields.
414 (**C**) Controls for immunohistological staining with normal IgG for Ni-DAB staining, AP staining or both
415 in the inferior frontal cortexes (IFCs) of non-COVID-19 autism cases and with an hACE2 antibody for
416 Ni-DAB staining.
417 Detection of the hACE2 receptor in neurons and nonneuronal cells in the IFCs of non-COVID-19 autism
418 cases. The hACE2-positive neurons are labeled with antibodies against NFL (**D**) or Tuj1 (**E**), the
419 oligodendrocyte marker CNPase (**F**), and the microglial marker Iba1 (**G**).
420 (**H**) hACE2 and cell marker double-positive cells were quantified (%, n $\geq$ 5 random fields).
421 SP positivity was detected in neurons and nonneuronal cells in the IFCs of the COVID-19 autism case (ID
422 #6437). SP-positive neurons labeled with Tuj1 (**I**), NeuN (**J**), the GABAergic inhibitory neuronal marker
423 GAD65 (**K**), the glutamatergic excitatory neuronal marker GS (glutamine synthetase) (**L**), the
424 oligodendrocyte marker CNPase (**M**), and the microglial marker Iba1 (**N**). $GFAP^+$ astrocytes were SP
425 negative (green arrows) (**O**).
426 (**P**) Quantification of SP and cell marker double positive cells (%, n $\geq$ 5 random fields).
427 AD: Alzheimer's disease; ASD: autism. Scale bar = 20 μm. In A and B, * indicate significant difference
428 ($P < 0.05$) by *t* test.

429 **Figure 3. Spike protein-positive cells undergo programmed cell death.**

430 Representative images of double SARS-CoV-2 spike protein (SP) (Ni-DAB staining: black signal) and
431 cleaved caspase 3 (cl-casp3; AP: red signal) staining in the cortexes of age-matched non-COVID-19
432 autism and COVID-19 autism cases (**A**) and non-COVID-19 Alzheimer's and the COVID-19 Alzheimer's
433 case (**B**). The inset boxes show cl-casp3 and SP double-labeled cells, cl-casp3-positive cells and double-
434 negative cells.

435 The graphs show the percentages of double SP^+ and cl-casp3^+ cells among total cleaved caspase 3^+ cells
436 in at least 5 random fields. * indicate significant difference ($P < 0.05$) compared with the non-COVID-19
437 controls by *t* test.

438 Representative images of SP staining with the necroptosis marker phospho-MLKL (**C**), the ferroptosis
439 marker TfR1 (**D**), and the senescence marker DPP4 (**E**) in the cortexes of the non-COVID-19 autism cases,
440 the COVID-19 Alzheimer's case and the two COVID-19 autism cases. Black arrows point to the double
441 SP^+ and cl-casp3^+ cells.

442 The graphs show the percentages of SP^+ necroptotic cells, ferroptotic cells and senescent cells counted
443 from at least 5 random fields ($n \geq 5$, in 2 COVID-19 ASD cases and 1 COVID-19 AD case). * indicate
444 significant difference ($P < 0.05$) compared with the non-COVID-19 controls by one-way ANOVA and
445 *Tukey* test. Scale bars = 20 μm.

446

447 **Figure 4. SARS-CoV-2 infection induces or enhances Aβ aggregate/plaque and p-Tau pretangles**
448 **formation.**

449 Aβ immunohistochemical staining (with the anti-Aβ antibody 6E10) in three cortical regions of two cases
450 of COVID-19 autism (**A**) and one case of COVID-19 with no underlying conditions (NUC) (**B**) and their
451 age-matched control cases. Cytoplasmic deposition of Aβ (blue arrows) was observed in COVID-19

452 autism (ASD) cortexes, and Aβ plaques (red arrow) were observed in the EC of one COVID-19 ASD case.
453 Immunofluorescence analysis with thioflavin-T indicated that the cytoplasmic deposits of Aβ in the
454 COVID-19 autism cortex consisted of aggregated Aβ (inset in **A,** upper panel most right). (**C**) Aβ
455 immunohistochemical staining in the cortical regions and hippocampi of the COVID-19 FTD and
456 Alzheimer's disease cases, and their age-matched controls. (**D**) Quantification of cellular Aβ aggregates
457 in ASD and NUC cases or Aβ plaques per mm^2 in FTD and AD cases (3 sections for each region and 3
458 independent images for one section). (**E**) p-Tau (pSer202) staining in the cortexes of COVID-19 ASD (E)
459 and COVID-19 NUC (**F**) cases and their age-matched controls. (**G**) p-Tau staining in the cortexes and
460 hippocampi of the two COVID-19 FTD and Alzheimer's disease cases and their age-matched controls.
461 (**H**) Quantification of cellular p-Tau deposition per mm^2 (3 sections for each region and 3 independent
462 images for one section). The two COVID-19 ASD cases showed p-Tau pretangle-like structures (indicated
463 by red arrows) and cytoplasmic p-Tau deposition (indicated by blue arrows). Increased/elevated Pick body
464 (red arrows) deposition was observed in the COVID-19 FTD case, and there were no differences in p-Tau
465 tangle numbers in AD cases. Entorhinal cortex: EC; inferior frontal cortex: IFC; dorsolateral prefrontal
466 cortex: DPC. Significant *P*-values are indicated (by Mann-Whitney U test after confirming a normal
467 distribution). Bars = 100 μm.

468 **Figure 5. SARS-CoV-2 infects mature neurons derived from human iPSCs.**

469 (**A**). SARS-CoV-2-GFP does not infect immature neurons at iPSC neuron differentiation day 35 (n = 3
470 replicates).

471 (**B**). Immature neurons do not express the mature neuron marker, NeuN.

472 (**C**). SARS-CoV-2 infects mature neurons at iPSC neuron differentiation day 50 (n = 3).

473 (**D**). Detection of SARS-CoV-2 in the culture medium of infected neurons (n = 3).

474 (**E**). SARS-CoV-2 infects Tuj1-positive neurons (n = 3).

475 (**F**). GFAP is not expressed in SARS-CoV-2-infected cells at iPSC differentiation day 50 (n = 2).

476 Immature Tuj1-positive neurons do not express ACE2 (**G**) and NRP1 (**H**) (n = 3).

477 Mature Tuj1 positive neurons express ACE2 (**I**) and NRP1 (**J**) (n = 3).

478 The bar graphs show the percentages of double Tuj1- and ACE2- or NRP1-positive cells (yellow) among

479 total $Tuj1^{+}$ cells (green) (n = 3). AD: Alzheimer's disease; CTL: control group (non-AD); ACE2:

480 angiotensin-converting enzyme 2; Tuj1: beta-Tubulin III; NRP1: Neuropilin 1; SPIKE: SARS-CoV-2

481 spike protein.

482 **Figure 6. SARS-CoV-2 induces or enhances Alzheimer's-like neuron phenotypes.**

483 (**A**). SARS-CoV-2 induces cellular Aβ aggregation in neurons derived from iPSCs of healthy individuals

484 and Alzheimer's patients (n = 3 iPSC lines).

485 (**B**). SARS-CoV-2 induces cellular p-Tau deposition in neurons derived from iPSCs of healthy individuals

486 and Alzheimer's patients (n = 3 iPSC lines).

487 The values in the graphs are presented as the means ± SEMs (n = 5 images from 2 independent experiments

488 for each group). The Aβ and p-Tau intensity data were analyzed by Mann-Whitney U test after confirming

489 a normal distribution. Bars = 50 μm.

490 mRNAs levels of inflammatory cytokines (**C**), BACE1 (**D**), and Alzheimer's molecular mediators (APP,

491 PSEN1 and PSEN2) (**E**) in SARS-CoV-2-infected neurons derived from iPSCs (n = 6, 3 iPSC lines for 2

492 independent experiments).

493 F. Cleaved caspase 3 (c-Cas3)-positive cells in SARS-CoV-2 infected neurons derived from iPSCs (n = 6

494 iPSC lines for 2 independent experiments). The bar graph shows the quantification of c-Cas3-positive cell

495 numbers. CTL: control group (iPSCs from healthy individuals); AD: Alzheimer's disease; CTLv: SARS-

496 CoV-2-infected control group; ADv: SARS-CoV-2-infected AD group; Tuj1: beta-Tubulin III; c-Cas3,

497 cleaved caspase 3. Data were analyzed by Mann-Whitney U test after confirming a normal distribution,

498 significant *P*-values are presented.

499 **Figure 7. Identification of an infectious etiology gene signature for Alzheimer's disease.**

500 (**A**). Volcano plot of differentially expressed genes (DEGs) in neurons derived from iPSCs of patients with
501 Alzheimer's disease (AD) (the AD group) compared to neurons derived from iPSCs of healthy individuals
502 (the CTL group).

503 (**B**). Volcano plot of DEGs in healthy individual iPSC-derived neurons infected with SARS-CoV-2 (the
504 CTL_V group) compared to the CTL group.

505 (**C**). Volcano plot of DEGs in AD neurons infected with SARS-CoV-2 (the AD_V group) compared to the
506 CTL group.

507 (**D**). Venn plot and KEGG pathway analysis for DEGs between the AD group and the CTL_V group. The
508 CTL group served as the baseline group. The twenty-four overlapping genes constituted the AD infectious
509 etiology gene signature.

510 (**E**). Venn plot and KEGG pathway analysis for DEGs between the AD group and the AD_V group. The
511 CTL group served as the baseline group.

512 For **A** to **E**, n = 3 iPSC lines for the CTL and AD groups.

513 (**F-G**). Analysis of the effect of siRNA mediated individual or combined knockdown of the top 3
514 downregulated genes, GJA8, CryAA2 and PSG6, on the AD infectious etiology gene signature in primary
515 human neurons. **F**: Immunoblot analysis of Aβ isoforms (n = 3 replicates). **G**. Cellular Aβ aggregation
516 (left panel) and cellular p-Tau deposition (right panel). Aβ aggregates and p-Tau accumulation in the
517 cytoplasm or neuronal axon are indicated by white arrowheads. The values in the graphs are presented as
518 the means ± SEMs (n = 8 images from 3 replicates). Intensity data were analyzed by Mann-Whitney U
519 test after confirming a normal distribution, significant *P*-values are presented. Scale bar, 50 μm.

520

521 **Supplemental figure titles and legends**

522 **Fig. S1. Presence of SARS-CoV-2 spike protein in cortical cells of five COVID-19 cases**.

523 Spike protein staining signals were visualized with an alkaline phosphatase (AP)-coupled goat anti-rabbit
524 secondary antibody and AP red substrate. SARS-CoV-2 spike protein red signals were located in the
525 cytosol of cortical cells of one COVID-19 autism (ASD) case but not in cells of an age-matched non-
526 COVID-19 ASD control (**A**). Spike protein (DAB staining, brown signal; counterstained with hematoxylin,
527 blue) was present in the cytosol of cortical cells of the COVID-19 FTD case (ID #5922) (**C**, three different
528 fields, arrows) but not in those of the age-matched non-COVID-19 FTD controls (**B,** 3 cases). In the
529 COVID-19 case without underlying conditions (ID #5932), the spike protein was also visible (**E,** three
530 different fields, arrows), but it was not visible in the age-matched non-COVID-19 AD controls (**D,** 3 cases).
531 RNAscope *in situ* hybridization showing COVID-19 genomic RNAs in four COVID-19 cases (**F**): 2 ASD
532 COVID-19 cases, 1 AD COVID-19 case, 1 FTD COVID-19 case, and 1 COVID-19 case without
533 underlying conditions. Scale bar = 20 μm.

534

535 **Fig. S2. Immunostaining of immune cell markers in brain tissues of COVID-19 patients.**

536 Immunolabeling (DAB, brown signal) with antibodies against CD3 (T cell marker, **A**), CD20 (B cell
537 marker, **B**), and F4/80 (macrophage marker, **C**) showed positively labeled immune cells in the cortex of
538 the COVID-19 Alzheimer's case. Immune cells were not detected in non-COVID-19 autism cases or the
539 two COVID-19 autism cases (**A-C**). Counterstaining: hematoxylin. The arrows point to immune cells. (**D**)
540 The percentages of immune cells were quantified from 3 sections (n = 3). * indicates a significant
541 difference ($P < 0.05$) by one-way ANOVA and Tukey's test. Scale bar = 20 μm.

542

543 **Fig. S3. Programmed cell death in SARS-CoV-2 spike protein positive-cortical cells.**

544 Representative images of cleaved caspase-3 staining (DAB, brown signal) in the cortexes of age-matched

545 non-COVID-19 autism cases, 2 COVID-19 autism cases, and 1 COVID-19 case with no underlying
546 conditions (**A**). Cleaved caspase-3-positive cells in the non-COVID-19 Alzheimer's, COVID-19
547 Alzheimer's, non-COVID-19 FTD, and COVID-19 FTD cases (**B**). Counterstaining: hematoxylin (blue).
548 (**C**) Quantification of cleaved caspase-3^+ cells in at least 5 random fields ($n \geq 5$, in 2 autism cases, 1 AD
549 case, 1 FTD case and 1 case without underlying conditions). The arrows point to cleaved caspase-3^+ (cl-
550 casp-3^+) cells. Representative images of spike protein-positive signals (black dots) with p-Ripk3^+
551 necroptotic cells (**D**) and ASCL4^+ ferroptotic cells (**E**) in the non-COVID-19, COVID-19 Alzheimer's
552 (AD), and COVID-19 autism (ASD) cases. The arrows point to the double-positive cells. Quantification
553 of double-positive cell numbers (spike protein and programmed cell death marker positive) from at least
554 5 random fields ($n \geq 5$). * indicates a significant difference ($P < 0.05$) compared with non-COVID-19
555 controls by one-way ANOVA and *Tukey's* test. Scale bar = 20 μm.
556
557 **Figure. S4. Cytokine expression in COVID-19 autism cortexes.**
558 Representative images of immunostaining of the cytokines IL-1β (**A**) and IL-6 (**B**) in the two cases of
559 COVID-19 autism (ASD) and in age-matched non-COVID-19 ASD controls (CTL) in the entorhinal
560 cortex (EC). (**C**) Quantification of immunostaining intensity (n = 6, 3 random fields per case per region).
561 Data were analyzed by Mann-Whitney U test after confirming a normal distribution, a significant *P*-value
562 is presented. Scale bar = 100 μm.
563
564 **Fig. S5. SARS-CoV-2 infects mature neurons derived from human iPSCs.**
565 (**A**) SARS-CoV-2-GFP does not infect immature neurons at iPSC differentiation day 35. White asterisks
566 (*) indicate nonspecific fluorescent signals. (**B**) Immature neurons do not express the mature neuron
567 marker NeuN. (**C**). SARS-CoV-2 infects mature neurons at iPSC differentiation day 50. (**D**). SARS-CoV-
568 2-GFP infects mature neurons at different dosages. CTL (non-AD: iPSCs derived from healthy

individuals): control groups; AD: Alzheimer's disease; Tuj1: beta-Tubulin III; SPIKE: SARS-CoV-2 spike protein.

Fig. S6. Effects of identified Alzheimer's infectious etiology genes on Aβ and p-Tau in human primary neurons. (**A**). Upregulated genes in AD neurons that were further upregulated due to SARS-CoV-2 infection. (**B**). Downregulated genes in AD neurons that were further downregulated due to SARS-CoV-2. (**C**). KEGG pathway analysis of the upregulated and downregulated genes in AD neurons that were further upregulated and downregulated by SARS-CoV-2. CTL (non-AD: iPSCs derived from healthy individuals): control groups; AD: Alzheimer's disease; ADV: SARS-CoV-2-infected AD group. For each group, n = 3.

(**D**) Immunofluorescence staining with the indicated antibodies after lentivirus-mediated overexpression of the top 3 upregulated genes, FCGR, LILRB5 and OTOR, identified in Fig. 7D as AD infectious etiology genes. Combined or individual overexpression of these three genes did not induce Aβ cellular aggregation, and only FCGR overexpression increased Tau phosphorylation at Ser202.

(**E**) Immunofluorescence staining of the indicated antibodies after siRNA-mediated knockdown of the top 3 downregulated genes, GJA8, CryAA2 and PSG6, identified in Fig. 7D as AD infectious etiology genes. Knockdown of GJA8, CryAA2 or PSG6 individually caused Aβ cellular aggregation and significantly increased Tau phosphorylation at Ser202.

588 **References**

589 1 Helms, J. *et al.* Neurologic Features in Severe SARS-CoV-2 Infection. *N Engl J Med* **382**, 2268-
590 2270, doi:10.1056/NEJMc2008597 (2020).
591 2 Mao, L. *et al.* Neurologic Manifestations of Hospitalized Patients With Coronavirus Disease 2019
592 in Wuhan, China. *JAMA Neurol* **77**, 683-690, doi:10.1001/jamaneurol.2020.1127 (2020).
593 3 de Erausquin, G. A. *et al.* The chronic neuropsychiatric sequelae of COVID-19: The need for a
594 prospective study of viral impact on brain functioning. *Alzheimers Dement*, doi:10.1002/alz.12255
595 (2021).
596 4 Taquet, M., Geddes, J. R., Husain, M., Luciano, S. & Harrison, P. J. 6-month neurological and
597 psychiatric outcomes in 236 379 survivors of COVID-19: a retrospective cohort study using
598 electronic health records. *Lancet Psychiatry* **8**, 416-427, doi:10.1016/S2215-0366(21)00084-5
599 (2021).
600 5 De Santis, G. SARS-CoV-2: A new virus but a familiar inflammation brain pattern. *Brain Behav*
601 *Immun* **87**, 95-96, doi:10.1016/j.bbi.2020.04.066 (2020).
602 6 Li, K. *et al.* Middle East Respiratory Syndrome Coronavirus Causes Multiple Organ Damage and
603 Lethal Disease in Mice Transgenic for Human Dipeptidyl Peptidase 4. *J Infect Dis* **213**, 712-722,
604 doi:10.1093/infdis/jiv499 (2016).
605 7 Netland, J., Meyerholz, D. K., Moore, S., Cassell, M. & Perlman, S. Severe acute respiratory
606 syndrome coronavirus infection causes neuronal death in the absence of encephalitis in mice
607 transgenic for human ACE2. *J Virol* **82**, 7264-7275, doi:10.1128/JVI.00737-08 (2008).
608 8 Meinhardt, J. *et al.* Olfactory transmucosal SARS-CoV-2 invasion as a port of central nervous
609 system entry in individuals with COVID-19. *Nat Neurosci* **24**, 168-175, doi:10.1038/s41593-020-
610 00758-5 (2021).
611 9 Montagne, A., Zhao, Z. & Zlokovic, B. V. Alzheimer's disease: A matter of blood-brain barrier
612 dysfunction? *J Exp Med* **214**, 3151-3169, doi:10.1084/jem.20171406 (2017).
613 10 Fiorentino, M. *et al.* Blood-brain barrier and intestinal epithelial barrier alterations in autism
614 spectrum disorders. *Mol Autism* **7**, 49, doi:10.1186/s13229-016-0110-z (2016).
615 11 Iadecola, C., Anrather, J. & Kamel, H. Effects of COVID-19 on the Nervous System. *Cell* **183**, 16-
616 27 e11, doi:10.1016/j.cell.2020.08.028 (2020).
617 12 Hoffmann, M. *et al.* SARS-CoV-2 Cell Entry Depends on ACE2 and TMPRSS2 and Is Blocked
618 by a Clinically Proven Protease Inhibitor. *Cell* **181**, 271-280 e278, doi:10.1016/j.cell.2020.02.052
619 (2020).
620 13 Butowt, R. & Bilinska, K. SARS-CoV-2: Olfaction, Brain Infection, and the Urgent Need for
621 Clinical Samples Allowing Earlier Virus Detection. *ACS Chem Neurosci* **11**, 1200-1203,
622 doi:10.1021/acschemneuro.0c00172 (2020).
623 14 Cantuti-Castelvetri, L. *et al.* Neuropilin-1 facilitates SARS-CoV-2 cell entry and infectivity.
624 *Science* **370**, 856-860, doi:10.1126/science.abd2985 (2020).
625 15 Vanacker, C. *et al.* Neuropilin-1 expression in GnRH neurons regulates prepubertal weight gain
626 and sexual attraction. *EMBO J* **39**, e104633, doi:10.15252/embj.2020104633 (2020).
627 16 Rogers, J. P. *et al.* Psychiatric and neuropsychiatric presentations associated with severe
628 coronavirus infections: a systematic review and meta-analysis with comparison to the COVID-19
629 pandemic. *Lancet Psychiatry* **7**, 611-627, doi:10.1016/S2215-0366(20)30203-0 (2020).
630 17 Varatharaj, A. *et al.* Neurological and neuropsychiatric complications of COVID-19 in 153
631 patients: a UK-wide surveillance study. *Lancet Psychiatry* **7**, 875-882, doi:10.1016/S2215-
632 0366(20)30287-X (2020).

18 Paterson, R. W. *et al.* The emerging spectrum of COVID-19 neurology: clinical, radiological and laboratory findings. *Brain* **143**, 3104-3120, doi:10.1093/brain/awaa240 (2020).

19 Kadono, Y. *et al.* A case of COVID-19 infection presenting with a seizure following severe brain edema. *Seizure* **80**, 53-55, doi:10.1016/j.seizure.2020.06.015 (2020).

20 Hosseini, A. A., Shetty, A. K., Sprigg, N., Auer, D. P. & Constantinescu, C. S. Delirium as a presenting feature in COVID-19: Neuroinvasive infection or autoimmune encephalopathy? *Brain Behav Immun* **88**, 68-70, doi:10.1016/j.bbi.2020.06.012 (2020).

21 Alkeridy, W. A. *et al.* A Unique Presentation of Delirium in a Patient with Otherwise Asymptomatic COVID-19. *J Am Geriatr Soc* **68**, 1382-1384, doi:10.1111/jgs.16536 (2020).

22 Jaywant, A. *et al.* Frequency and profile of objective cognitive deficits in hospitalized patients recovering from COVID-19. *Neuropsychopharmacology*, doi:10.1038/s41386-021-00978-8 (2021).

23 Heneka, M. T., Golenbock, D., Latz, E., Morgan, D. & Brown, R. Immediate and long-term consequences of COVID-19 infections for the development of neurological disease. *Alzheimers Res Ther* **12**, 69, doi:10.1186/s13195-020-00640-3 (2020).

24 Vallamkondu, J. *et al.* SARS-CoV-2 pathophysiology and assessment of coronaviruses in CNS diseases with a focus on therapeutic targets. *Biochim Biophys Acta Mol Basis Dis* **1866**, 165889, doi:10.1016/j.bbadis.2020.165889 (2020).

25 Wang, Q., Davis, P. B., Gurney, M. E. & Xu, R. COVID-19 and dementia: Analyses of risk, disparity, and outcomes from electronic health records in the US. *Alzheimers Dement*, doi:10.1002/alz.12296 (2021).

26 Coil, D. A. *et al.* SARS-CoV-2 detection and genomic sequencing from hospital surface samples collected at UC Davis. *PLoS One* **16**, e0253578, doi:10.1371/journal.pone.0253578 (2021).

27 Gomez-Isla, T. *et al.* Neuronal loss correlates with but exceeds neurofibrillary tangles in Alzheimer's disease. *Ann Neurol* **41**, 17-24, doi:10.1002/ana.410410106 (1997).

28 Giannakopoulos, P. *et al.* Tangle and neuron numbers, but not amyloid load, predict cognitive status in Alzheimer's disease. *Neurology* **60**, 1495-1500, doi:10.1212/01.wnl.0000063311.58879.01 (2003).

29 Hou, Y. J. *et al.* SARS-CoV-2 Reverse Genetics Reveals a Variable Infection Gradient in the Respiratory Tract. *Cell* **182**, 429-446 e414, doi:10.1016/j.cell.2020.05.042 (2020).

30 Tian, J. H. *et al.* SARS-CoV-2 spike glycoprotein vaccine candidate NVX-CoV2373 immunogenicity in baboons and protection in mice. *Nat Commun* **12**, 372, doi:10.1038/s41467-020-20653-8 (2021).

31 Readhead, B. *et al.* Multiscale Analysis of Independent Alzheimer's Cohorts Finds Disruption of Molecular, Genetic, and Clinical Networks by Human Herpesvirus. *Neuron* **99**, 64-82 e67, doi:10.1016/j.neuron.2018.05.023 (2018).

32 Cairns, D. M. *et al.* A 3D human brain-like tissue model of herpes-induced Alzheimer's disease. *Sci Adv* **6**, eaay8828, doi:10.1126/sciadv.aay8828 (2020).

33 Song, E. *et al.* Neuroinvasion of SARS-CoV-2 in human and mouse brain. *J Exp Med* **218**, doi:10.1084/jem.20202135 (2021).

34 Thakur, K. T. *et al.* COVID-19 neuropathology at Columbia University Irving Medical Center/New York Presbyterian Hospital. *Brain*, doi:10.1093/brain/awab148 (2021).

35 Arbour, N., Day, R., Newcombe, J. & Talbot, P. J. Neuroinvasion by human respiratory coronaviruses. *J Virol* **74**, 8913-8921, doi:10.1128/jvi.74.19.8913-8921.2000 (2000).

36 Bullen, C. K. *et al.* Infectability of human BrainSphere neurons suggests neurotropism of SARS-CoV-2. *ALTEX* **37**, 665-671, doi:10.14573/altex.2006111 (2020).

37 Zhang, B. Z. *et al.* SARS-CoV-2 infects human neural progenitor cells and brain organoids. *Cell Res* **30**, 928-931, doi:10.1038/s41422-020-0390-x (2020).
38 Puelles, V. G. *et al.* Multiorgan and Renal Tropism of SARS-CoV-2. *N Engl J Med* **383**, 590-592, doi:10.1056/NEJMc2011400 (2020).
39 Pellegrini, L. *et al.* SARS-CoV-2 Infects the Brain Choroid Plexus and Disrupts the Blood-CSF Barrier in Human Brain Organoids. *Cell Stem Cell* **27**, 951-961 e955, doi:10.1016/j.stem.2020.10.001 (2020).
40 Alexopoulos, H. *et al.* Anti-SARS-CoV-2 antibodies in the CSF, blood-brain barrier dysfunction, and neurological outcome: Studies in 8 stuporous and comatose patients. *Neurol Neuroimmunol Neuroinflamm* **7**, doi:10.1212/NXI.0000000000000893 (2020).
41 Buzhdygan, T. P. *et al.* The SARS-CoV-2 spike protein alters barrier function in 2D static and 3D microfluidic in-vitro models of the human blood-brain barrier. *Neurobiol Dis* **146**, 105131, doi:10.1016/j.nbd.2020.105131 (2020).
42 Jacob, F. *et al.* Human Pluripotent Stem Cell-Derived Neural Cells and Brain Organoids Reveal SARS-CoV-2 Neurotropism Predominates in Choroid Plexus Epithelium. *Cell Stem Cell* **27**, 937-950 e939, doi:10.1016/j.stem.2020.09.016 (2020).
43 Ramani, A. *et al.* SARS-CoV-2 targets neurons of 3D human brain organoids. *EMBO J* **39**, e106230, doi:10.15252/embj.2020106230 (2020).
44 Lee, S. *et al.* Virus-induced senescence is driver and therapeutic target in COVID-19. *Nature*, doi:10.1038/s41586-021-03995-1 (2021).
45 Sun, X. *et al.* Hypoxia facilitates Alzheimer's disease pathogenesis by up-regulating BACE1 gene expression. *Proc Natl Acad Sci U S A* **103**, 18727-18732, doi:10.1073/pnas.0606298103 (2006).
46 Gordon, D. E. *et al.* A SARS-CoV-2 protein interaction map reveals targets for drug repurposing. *Nature* **583**, 459-468, doi:10.1038/s41586-020-2286-9 (2020).

Fig. 1

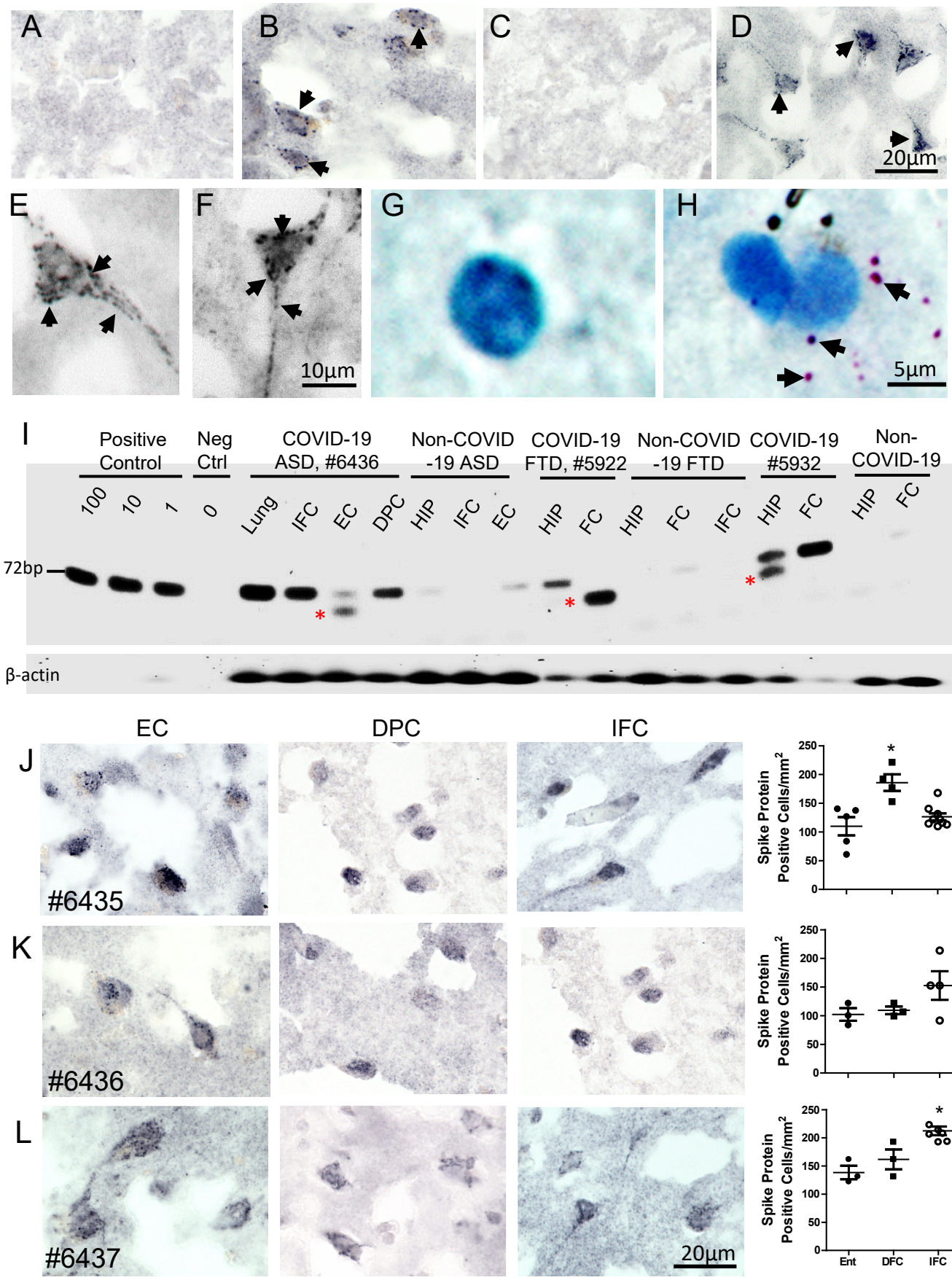
A
B
C
D
20µm
E
F
10µm
G
H
5µm
I
Positive Control
Neg Ctrl
COVID-19 ASD, #6436
Non-COVID -19 ASD
COVID-19 FTD, #5922
Non-COVID -19 FTD
COVID-19 #5932
Non-COVID-19
100
10
1
0
Lung
IFC
EC
DPC
HIP
IFC
EC
HIP
FC
HIP
FC
IFC
HIP
FC
HIP
FC
72bp
β-actin
EC
DPC
IFC
J
#6435
K
#6436
L
#6437
20µm
Spike Protein Positive Cells/mm²
250
200
150
100
50
0
Ent
DFC
IFC

Fig. 2

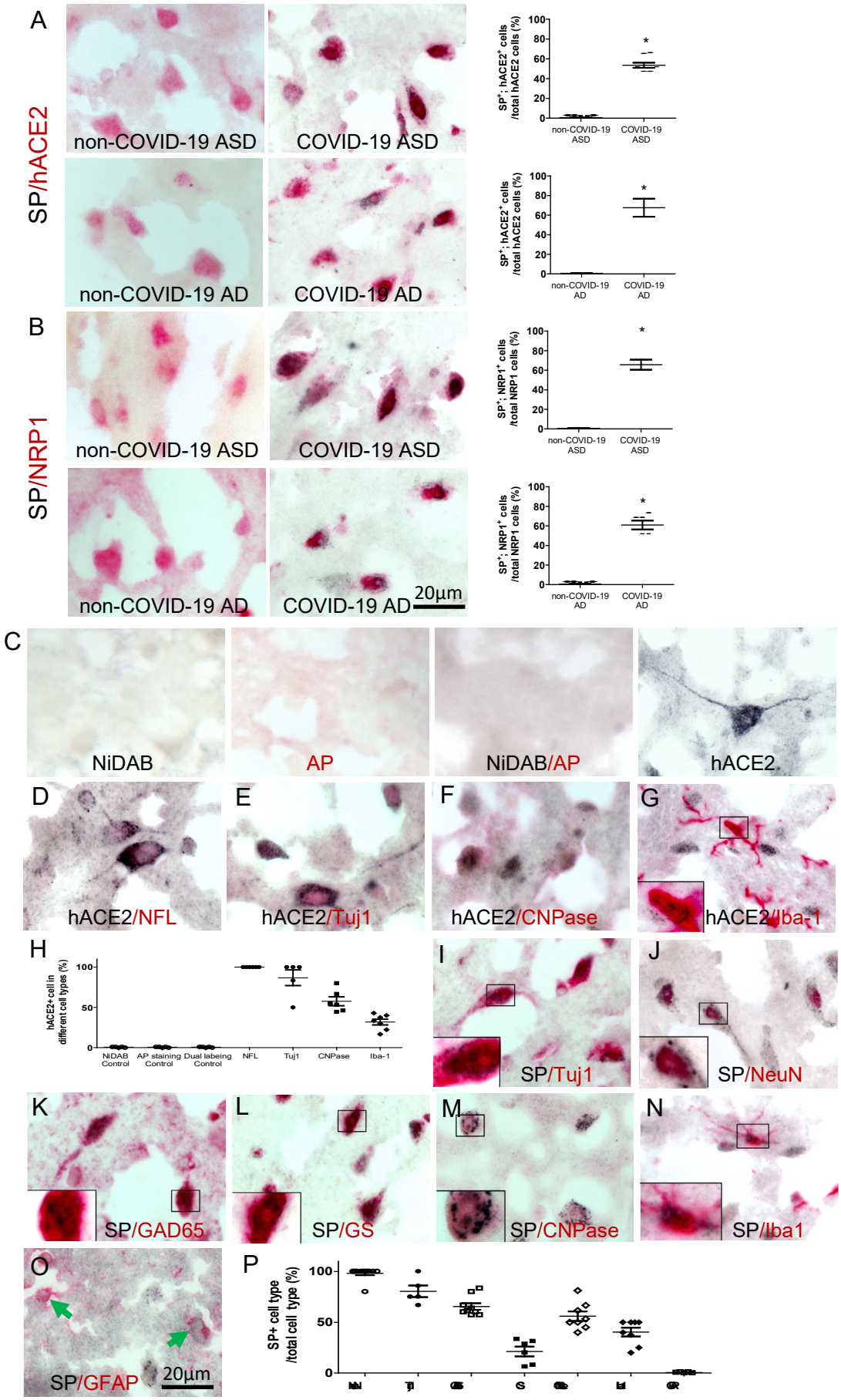
A
SP/hACE2
non-COVID-19 ASD
COVID-19 ASD
non-COVID-19 AD
COVID-19 AD
SP+; hACE2+ cells /total hACE2 cells (%)
B
SP/NRP1
SP+; NRP1+ cells /total NRP1 cells (%)
20μm
C
NiDAB
AP
NiDAB/AP
hACE2
D
hACE2/NFL
E
hACE2/Tuj1
F
hACE2/CNPase
G
hACE2/Iba-1
H
hACE2+ cell in different cell types (%)
NiDAB Control
AP staining Control
Dual labeing Control
NFL
Tuj1
CNPase
Iba-1
I
SP/Tuj1
J
SP/NeuN
K
SP/GAD65
L
SP/GS
M
SP/CNPase
N
SP/Iba1
O
SP/GFAP
20μm
P
SP+ cell type /total cell type (%)

Fig. 3

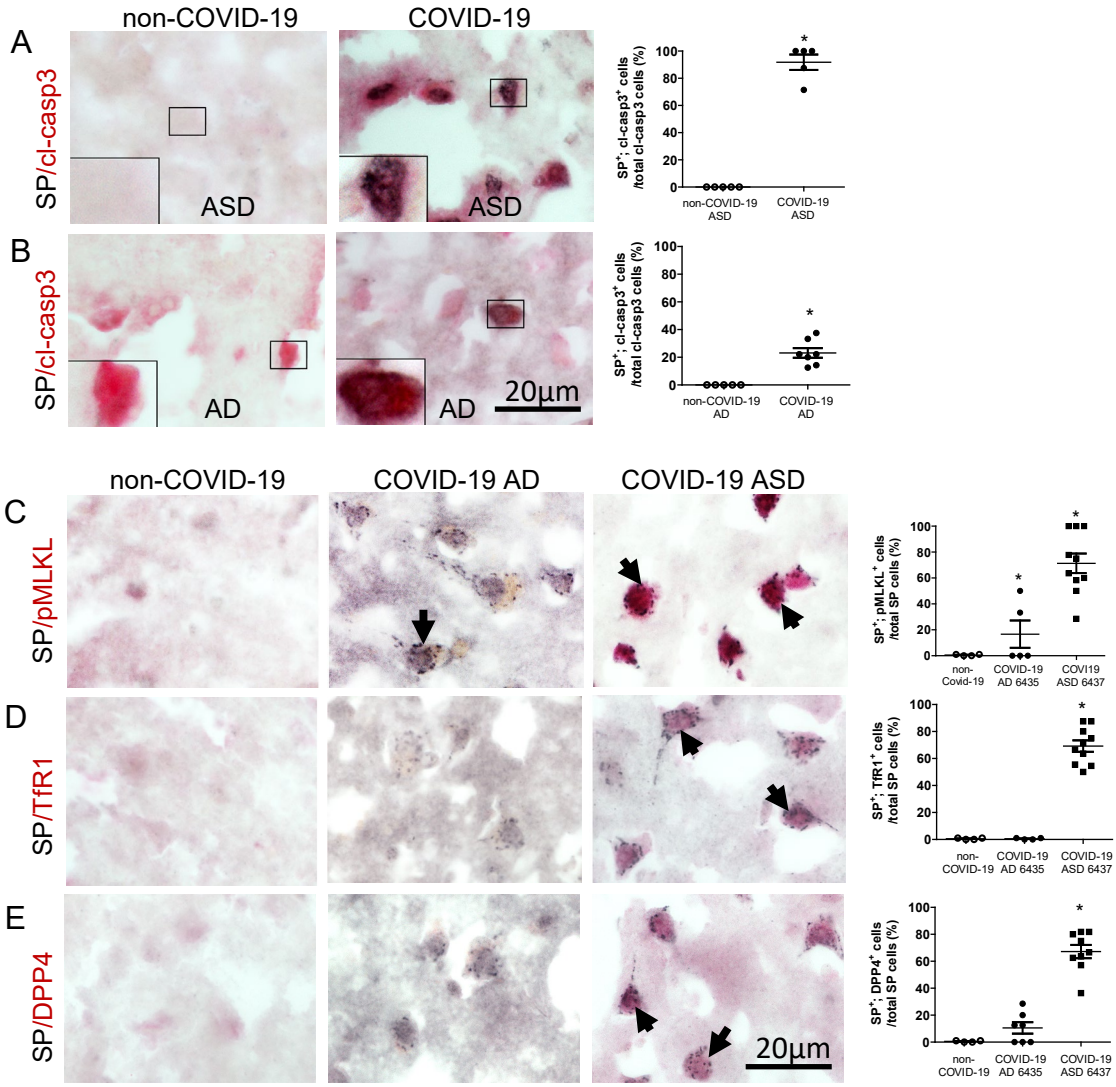
non-COVID-19
COVID-19
A
SP/cl-casp3
ASD
ASD
SP+; cl-casp3+ cells /total cl-casp3 cells (%)
non-COVID-19 ASD
COVID-19 ASD
B
SP/cl-casp3
AD
AD
20µm
non-COVID-19 AD
COVID-19 AD
non-COVID-19
COVID-19 AD
COVID-19 ASD
C
SP/pMLKL
SP+; pMLKL+ cells /total SP cells (%)
non-Covid-19
COVID-19 AD 6435
COVI19 ASD 6437
D
SP/TfR1
SP+; TfR1+ cells /total SP cells (%)
non-COVID-19
COVID-19 AD 6435
COVID-19 ASD 6437
E
SP/DPP4
20µm
SP+; DPP4+ cells /total SP cells (%)
non-COVID-19
COVID-19 AD 6435
COVID-19 ASD 6437

Fig. 4

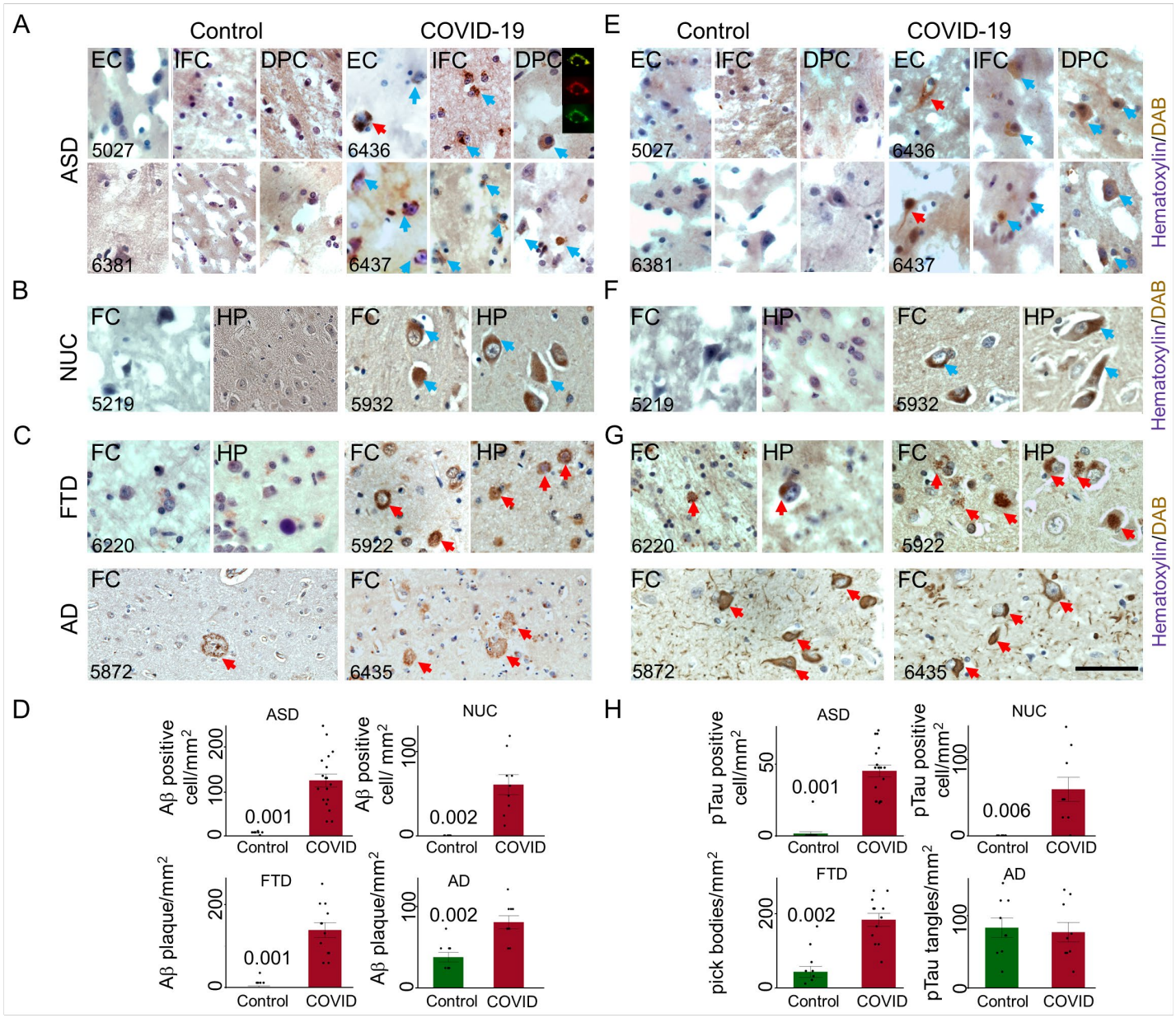
A
Control
COVID-19
EC
IFC
DPC
ASD
5027
6381
6436
6437
B
NUC
FC
HP
5219
5932
C
FTD
6220
5922
AD
5872
6435
E
F
G
Hematoxylin/DAB
D
Aβ positive cell/mm2
Aβ plaque/mm2
ASD
NUC
FTD
AD
0.001
0.002
Control
COVID
H
pTau positive cell/mm2
pick bodies/mm2
pTau tangles/mm2
0.006

Fig. 5

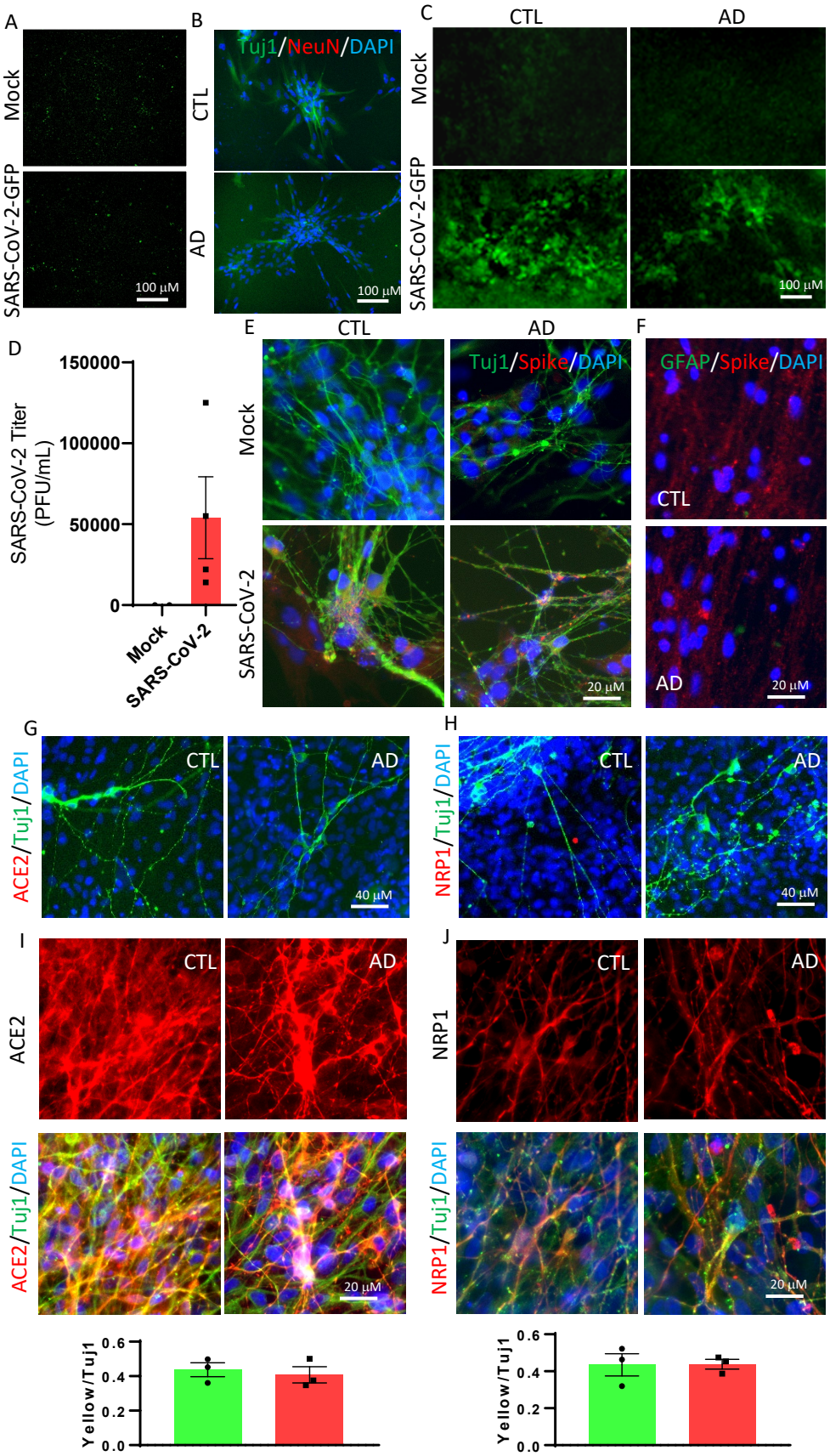
A
Mock
SARS-CoV-2-GFP
100 µM
B
Tuj1/NeuN/DAPI
CTL
AD
100 µM
C
CTL
AD
Mock
SARS-CoV-2-GFP
100 µM
D
SARS-CoV-2 Titer (PFU/mL)
150000
100000
50000
0
Mock
SARS-CoV-2
E
CTL
AD
Tuj1/Spike/DAPI
Mock
SARS-CoV-2
20 µM
F
GFAP/Spike/DAPI
CTL
AD
20 µM
G
ACE2/Tuj1/DAPI
CTL
AD
40 µM
H
NRP1/Tuj1/DAPI
CTL
AD
40 µM
I
ACE2
CTL
AD
ACE2/Tuj1/DAPI
20 µM
J
NRP1
CTL
AD
NRP1/Tuj1/DAPI
20 µM
Yellow/Tuj1
0.6
0.4
0.2
0.0
Yellow/Tuj1
0.6
0.4
0.2
0.0

Fig. 6

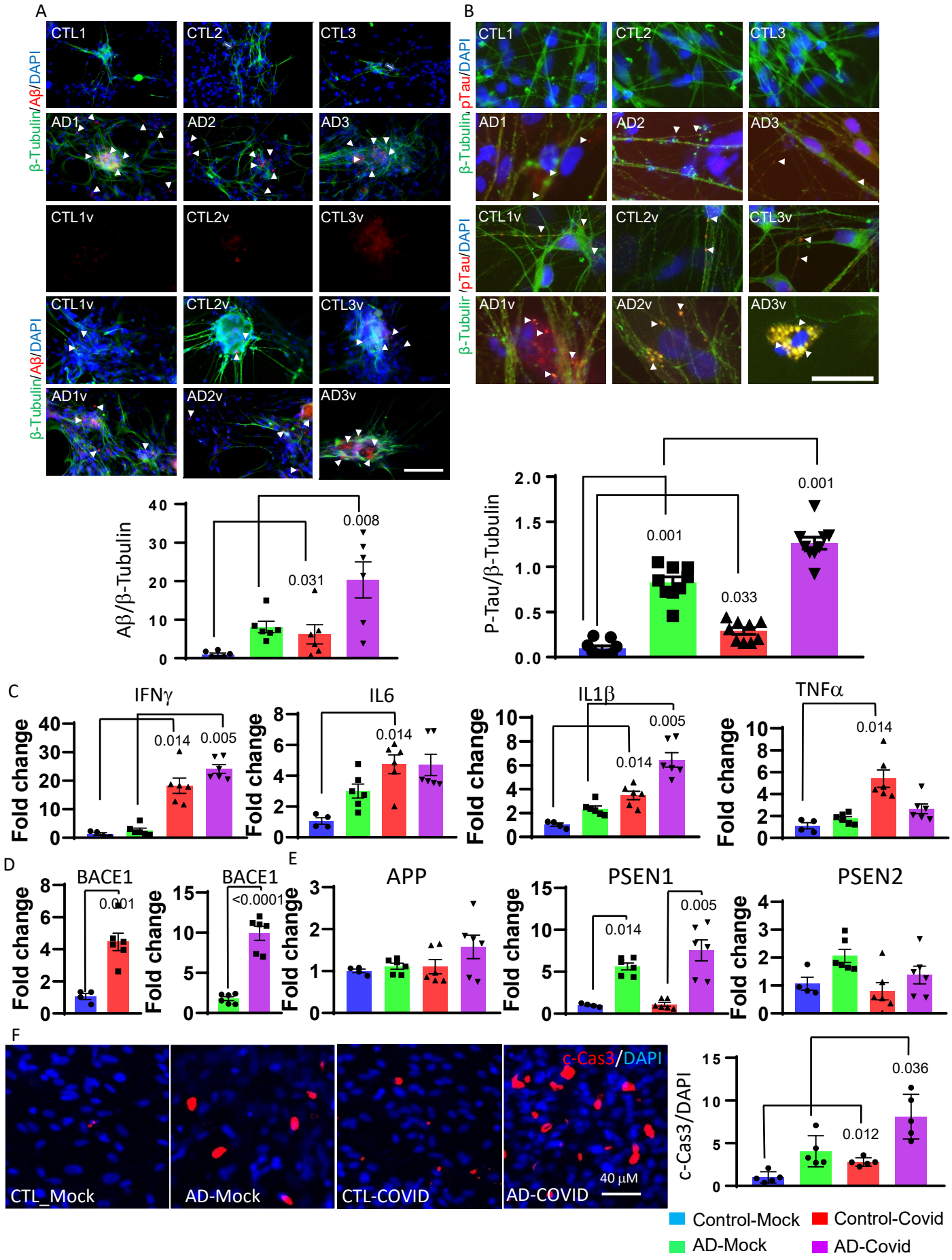
A
β-Tubulin/Aβ/DAPI
CTL1
CTL2
CTL3
AD1
AD2
AD3
CTL1v
CTL2v
CTL3v
AD1v
AD2v
AD3v
B
β-Tubulin/pTau/DAPI
Aβ/β-Tubulin
0.008
0.031
P-Tau/β-Tubulin
0.001
0.001
0.033
C
IFNγ
IL6
IL1β
TNFα
Fold change
0.014
0.005
D
BACE1
0.001
<0.0001
E
APP
PSEN1
PSEN2
F
c-Cas3/DAPI
CTL_Mock
AD-Mock
CTL-COVID
AD-COVID
40 μM
0.036
0.012
Control-Mock
Control-Covid
AD-Mock
AD-Covid

Fig. 7

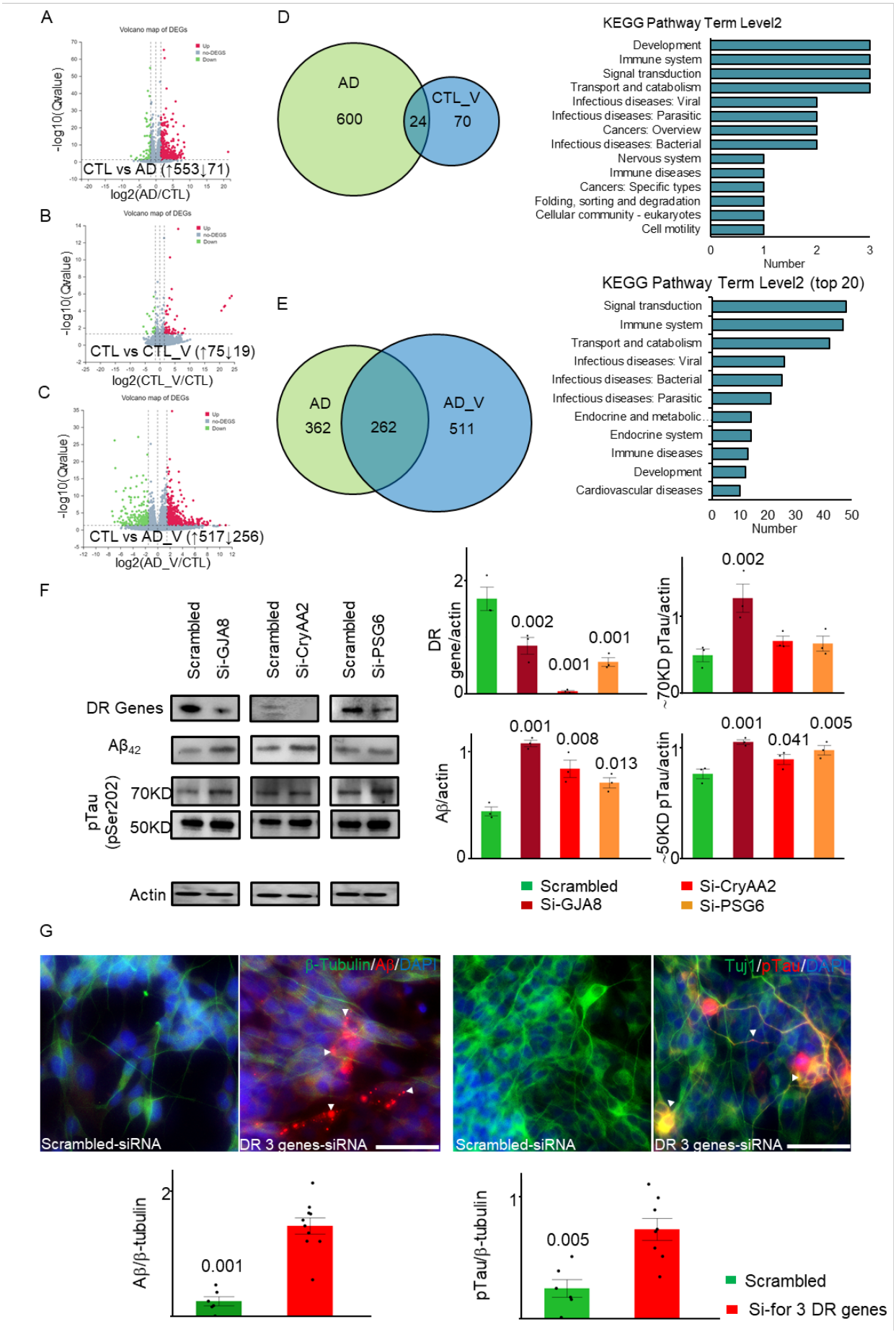
A
Volcano map of DEGs
Up
no-DEGS
Down
-log10(Qvalue)
CTL vs AD (↑553↓71)
log2(AD/CTL)
B
Volcano map of DEGs
-log10(Qvalue)
CTL vs CTL_V (↑75↓19)
log2(CTL_V/CTL)
C
Volcano map of DEGs
-log10(Qvalue)
CTL vs AD_V (↑517↓256)
log2(AD_V/CTL)
D
AD
600
24
CTL_V
70
KEGG Pathway Term Level2
Development
Immune system
Signal transduction
Transport and catabolism
Infectious diseases: Viral
Infectious diseases: Parasitic
Cancers: Overview
Infectious diseases: Bacterial
Nervous system
Immune diseases
Cancers: Specific types
Folding, sorting and degradation
Cellular community - eukaryotes
Cell motility
Number
E
AD
362
262
AD_V
511
KEGG Pathway Term Level2 (top 20)
Signal transduction
Immune system
Transport and catabolism
Infectious diseases: Viral
Infectious diseases: Bacterial
Infectious diseases: Parasitic
Endocrine and metabolic..
Endocrine system
Immune diseases
Development
Cardiovascular diseases
Number
F
Scrambled
Si-GJA8
Scrambled
Si-CryAA2
Scrambled
Si-PSG6
DR Genes
Aβ42
pTau (pSer202)
70KD
50KD
Actin
DR gene/actin
0.002
0.001
0.001
~70KD pTau/actin
0.002
Aβ/actin
0.001
0.008
0.013
~50KD pTau/actin
0.001
0.041
0.005
Scrambled
Si-GJA8
Si-CryAA2
Si-PSG6
G
β-Tubulin/Aβ/DAPI
Scrambled-siRNA
DR 3 genes-siRNA
Tuj1/pTau/DAPI
Scrambled-siRNA
DR 3 genes-siRNA
Aβ/β-tubulin
0.001
pTau/β-tubulin
0.005
Scrambled
Si-for 3 DR genes

Fig. S1

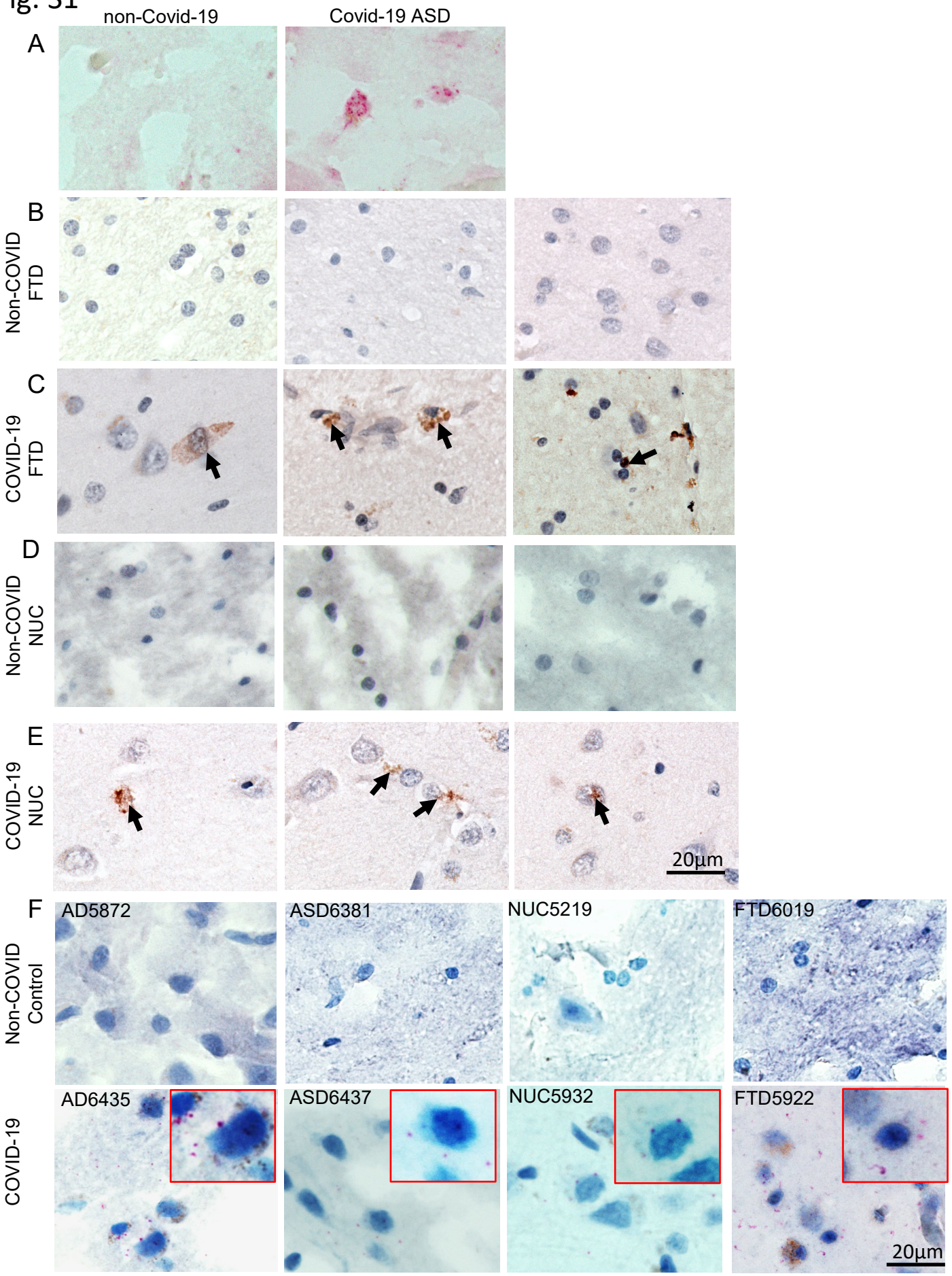
non-Covid-19
Covid-19 ASD
A
B
Non-COVID
FTD
C
COVID-19
FTD
D
Non-COVID
NUC
E
COVID-19
NUC
20µm
F
AD5872
ASD6381
NUC5219
FTD6019
Non-COVID
Control
AD6435
ASD6437
NUC5932
FTD5922
COVID-19
20µm

Fig. S2

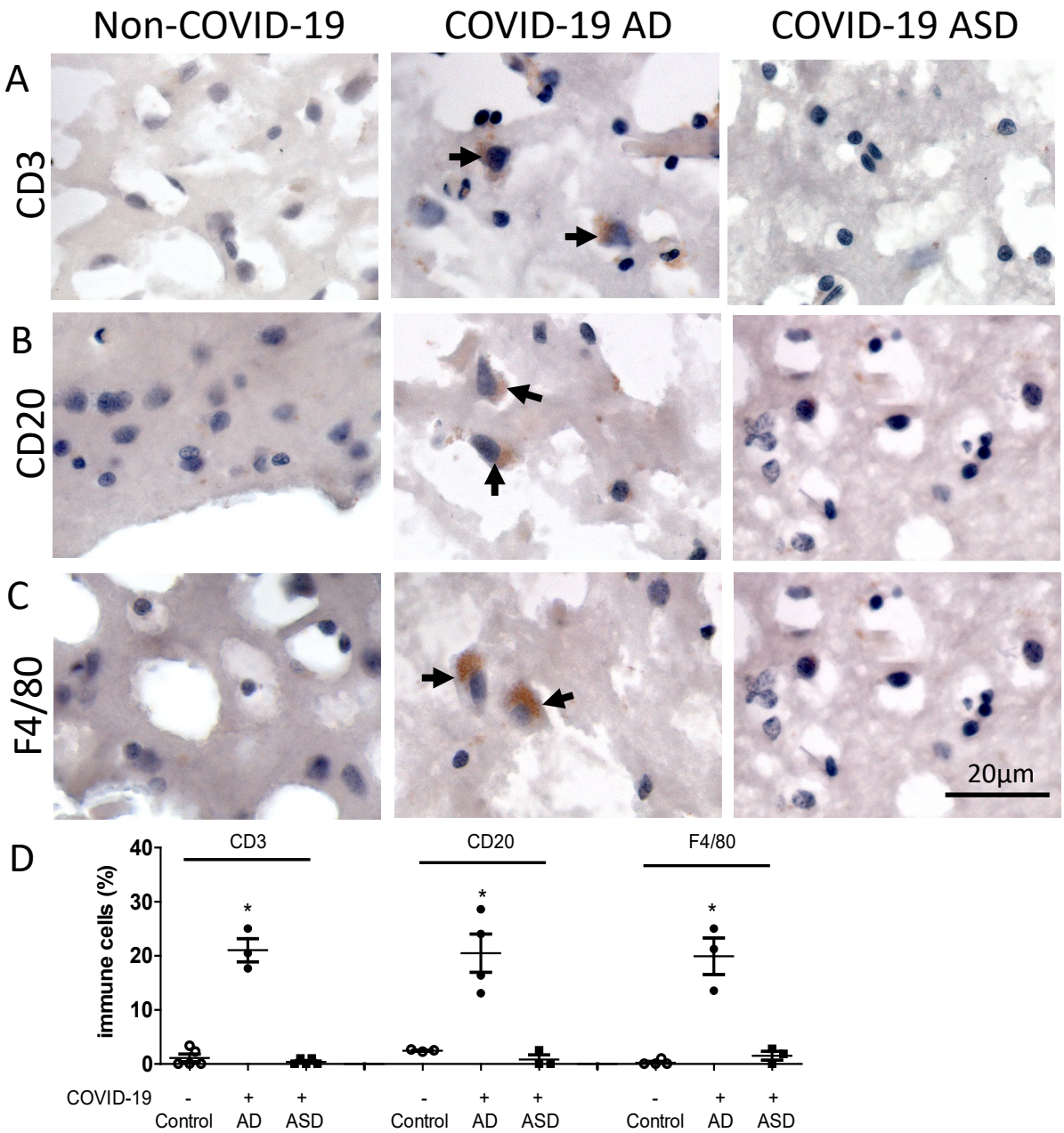
Non-COVID-19
COVID-19 AD
COVID-19 ASD
A
CD3
B
CD20
C
F4/80
20µm
D
CD3
CD20
F4/80
immune cells (%)
40
30
20
10
0
*
COVID-19
-
+
+
Control
AD
ASD

Fig. S3

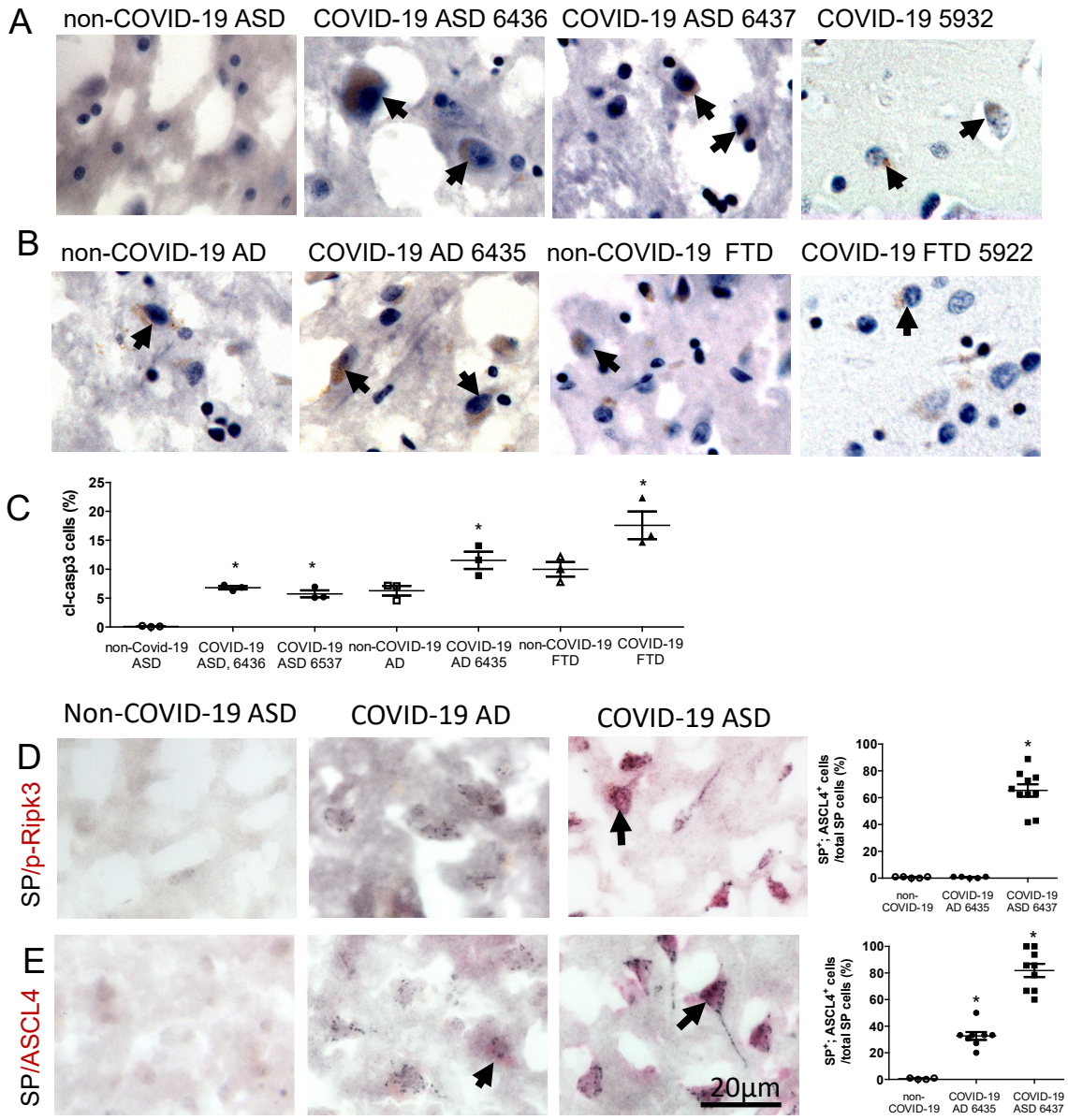
A
non-COVID-19 ASD
COVID-19 ASD 6436
COVID-19 ASD 6437
COVID-19 5932
B
non-COVID-19 AD
COVID-19 AD 6435
non-COVID-19 FTD
COVID-19 FTD 5922
C
cl-casp3 cells (%)
25
20
15
10
5
0
non-Covid-19 ASD
COVID-19 ASD, 6436
COVID-19 ASD 6537
non-COVID-19 AD
COVID-19 AD 6435
non-COVID-19 FTD
COVID-19 FTD
Non-COVID-19 ASD
COVID-19 AD
COVID-19 ASD
D
SP/p-Ripk3
SP+; ASCL4+ cells /total SP cells (%)
100
80
60
40
20
0
non-COVID-19
COVID-19 AD 6435
COVID-19 ASD 6437
E
SP/ASCL4
SP+; ASCL4+ cells /total SP cells (%)
100
80
60
40
20
0
non-COVID-19
COVID-19 AD 6435
COVID-19 ASD 6437
20µm

Fig. S4

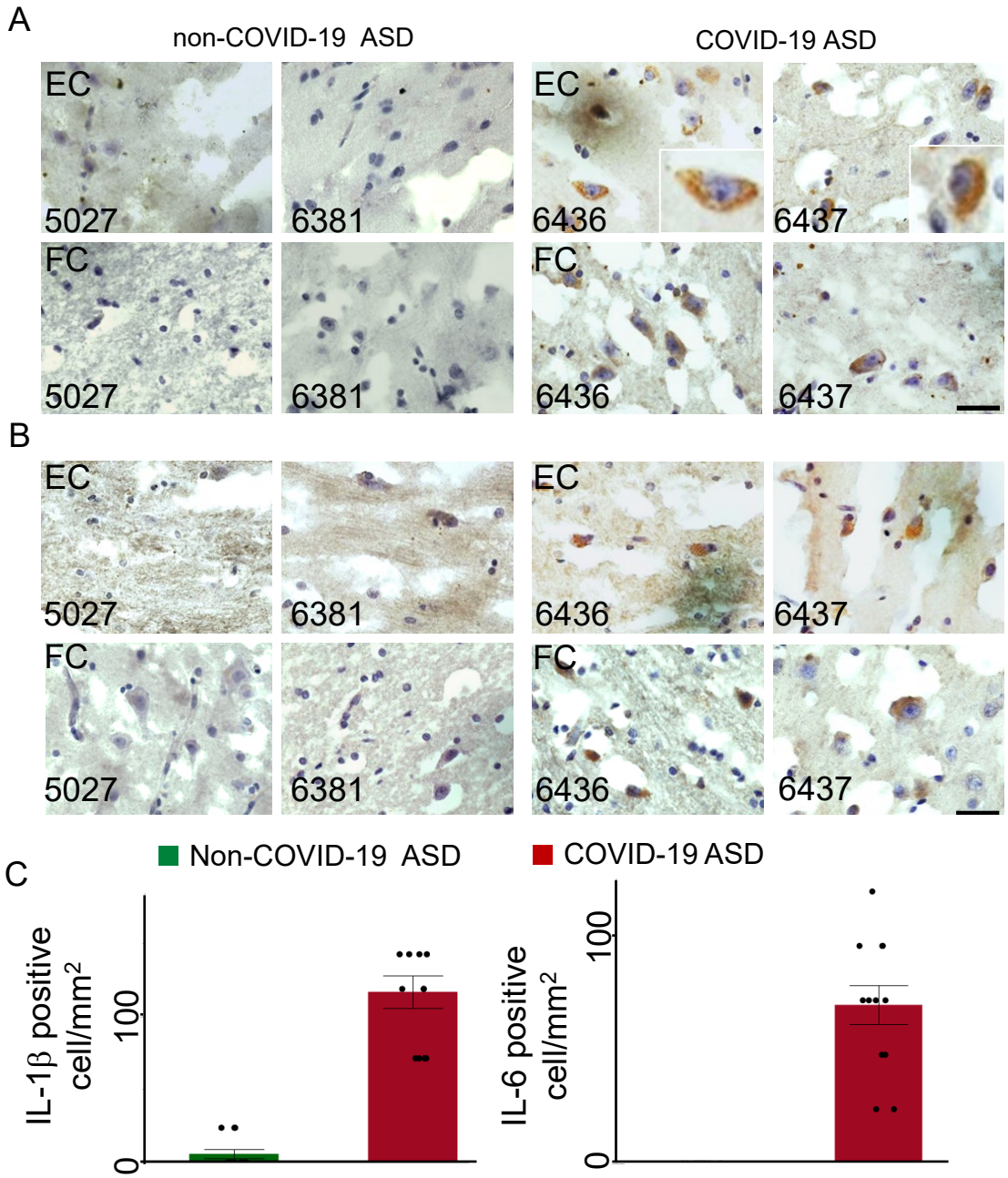
A
non-COVID-19 ASD
COVID-19 ASD
EC
5027
6381
6436
6437
FC
B
C
Non-COVID-19 ASD
COVID-19 ASD
IL-1β positive cell/mm2
IL-6 positive cell/mm2
100
0

Fig. S5

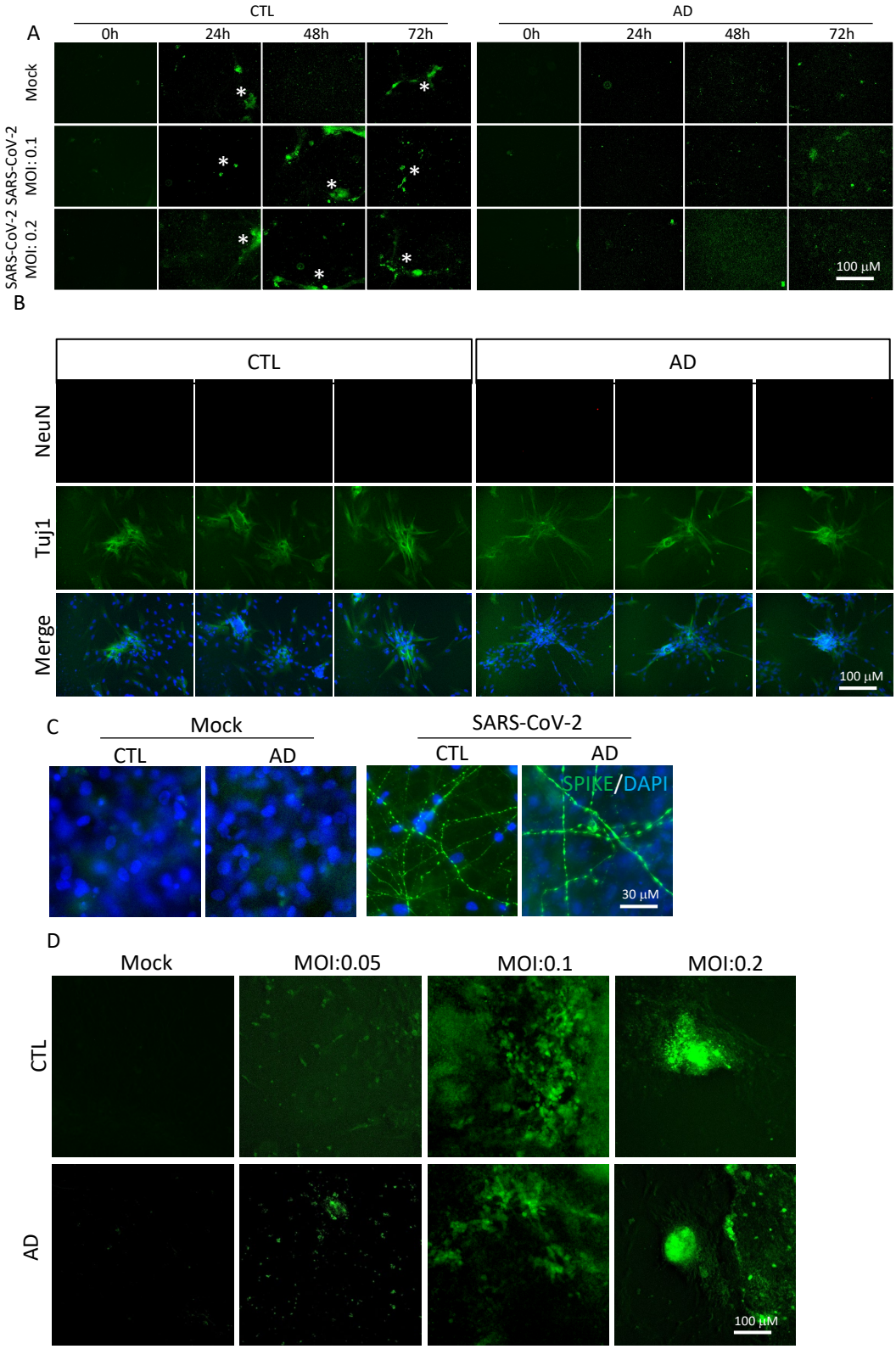
A
CTL
AD
0h
24h
48h
72h
Mock
SARS-CoV-2 MOI: 0.1
SARS-CoV-2 MOI: 0.2
100 µM
B
CTL
AD
NeuN
Tuj1
Merge
100 µM
C
Mock
SARS-CoV-2
CTL
AD
SPIKE/DAPI
30 µM
D
Mock
MOI:0.05
MOI:0.1
MOI:0.2
CTL
AD
100 µM

Fig. S6

A

Gene	CTL/AD	CTL/AD_V
XAF1	1.60	3.58
TWIST2	1.81	3.96
CASP4	1.55	3.17
CD34	1.82	3.54
CCL4	2.83	5.49
CCL3	3.40	6.44
KLHDC7B	1.79	3.33
LILRB1	4.37	8.12
GJB2	1.84	3.40
LAIR1	1.92	3.38
PLA2G7	2.08	3.66
C3	2.31	4.05
FIBIN	1.67	2.85
HCK	1.99	3.36
SP140L	1.60	2.68
COMP	1.69	2.83
SLC22A4	1.53	2.53
LRRC25	2.42	3.91
CTSS	2.38	3.78
SLAMF8	2.16	3.36
FERMT3	3.28	5.09
NPL	1.55	2.38
ITGAL	2.83	4.32
AOAH	2.29	3.48
CCL3L1	5.34	8.10

Deteriorated fold > 1.5
Upregulated genes

B

Gene	CTL/AD	CTL/AD_V
PLA2G2F	-1.58	-5.46
CRYAA2	-1.88	-5.82
ABCB11	-1.65	-4.64
GJA8	-1.81	-5.06
CRYBB3	-1.76	-4.11
CRYBB1	-2.58	-5.90
C1orf105	-1.65	-3.70
CRYBA1	-2.68	-6.02
MIP	-3.11	-6.95
CRYBA4	-2.58	-5.66
GPD1	-1.60	-3.43
BHMT	-2.52	-5.31
PITX3	-2.07	-4.33
CRYBA2	-3.24	-6.72
GJA3	-1.63	-3.38
CRYGS	-2.73	-5.65
PSG7	-3.39	-6.95
PSG3	-3.17	-6.45
KMO	-1.78	-3.62
PSG2	-3.57	-7.24
CRYGD	-1.83	-3.70
CRYAB	-2.33	-4.53
CRYBB2	-2.84	-5.46
HSD3B1	-1.60	-2.96
PROX1	-1.67	-2.99
VIT	-1.68	-2.99
ERICH5	-1.59	-2.80
AQP5	-1.70	-2.96
PSG1	-2.66	-4.61
COLGALT2	-1.56	-2.61
CRYGC	-2.69	-4.45
ANKRD34C	-2.56	-4.18
DBX2	-2.75	-4.29
MAMDC2	-1.68	-2.54

C

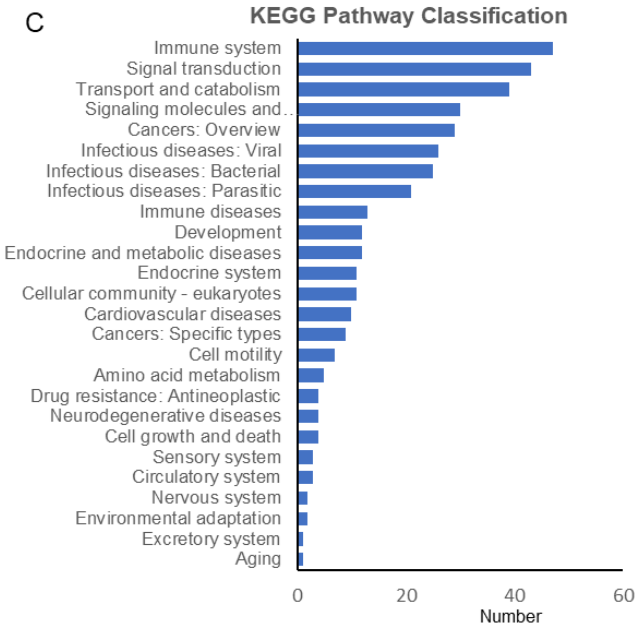

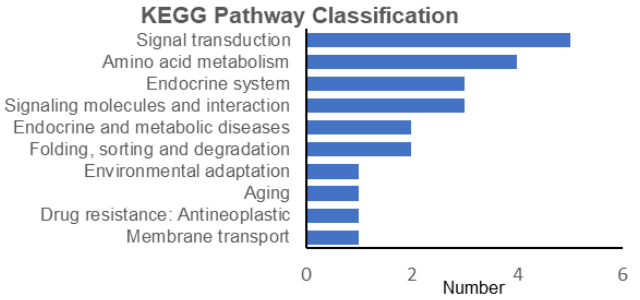

D

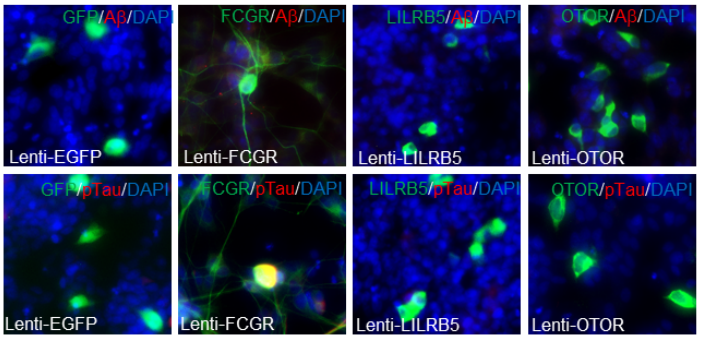

E

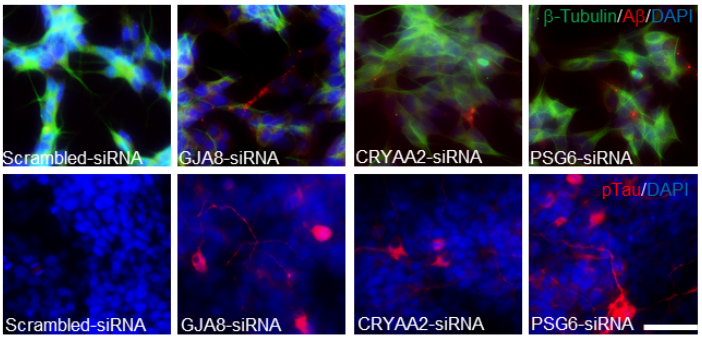

Table S1. Relative numbers of spike protein$^+$ cells in 5 COVID-19 cases

ID#	Disease	Age	EC	DPC	IFC
6435	COVID-19, AD	77	++	++	++
6436	COVID-19, ASD	38	++	++	++
6437	COVID-19, ASD	30	++	++	+++
5932	COVID-19, NUC	71	Not tested	Not tested	+
5922	COVID-19, FTD	70	Not tested	Not tested	+

AD: Alzheimer's disease; ASD: autism; EC: entorhinal cortex; DPC: dorsolateral prefrontal cortex; IFC: inferior frontal cortex. FTD: frontotemporal dementia. NUC: no underlying condition. +++: >200 spike protein$^+$ cells/mm^2; ++: 100-200 spike protein$^+$ cells/mm^2; +: <100 spike protein$^+$ cells/mm^2

Methods

Mammalian iPSCs and culture conditions

Human iPSCs (1 cases of familial AD, 2 cases of sporadic AD, and 3 cases of apparently healthy controls) purchased from the Coriell Institute for Medical Research were used in our study. iPSCs were maintained on irradiated mouse CF-1 feeder layer (ATCC, Manassas, VA) at 37 ºC and 5% CO_2 in Knockout DMEM medium (Invitrogen, Waltham, MA) supplemented with 20% Knockout Serum Replacer (KSR) (Invitrogen, Waltham, MA), 0.1 mM nonessential amino acids (Invitrogen, Waltham, MA), 2 mM GlutaMAX (Invitrogen, Waltham, MA), 0.1 mM β-Mercaptoethanol (Sigma-Aldrich, St. Louis, MO), 10 ng/ml recombinant human basic fibroblast growth factor (Invitrogen, Waltham, MA) (hiPSC medium).

Viral strains

Vero E6 cells were maintained in EMEM (ATCC) media with 10% Serum Plus II Medium Supplement (Sigma-Aldrich). SARS-CoV-2 virus were obtained from the CDC following isolation from a patient in Washington State (WA-1 strain - BEI #NR-52281). SARS-CoV-2 GFP was generously provided by Dr. Ralph S. Baric. Stocks were prepared by infection of Vero E6 cells.

Brain Tissues

The major source for postmortem tissues is the Brain and Tissue Bank at University of Maryland (UMB). The Brain and Tissue Bank is a brain and tissue repository of the NIH NeuroBioBank. The Brain Tissue Bank is a national resource for investigators utilizing human post-mortem brain tissues and related biospecimens for research in understanding the conditions of the nervous system. All brain tissue is procured, stored, and distributed according to applicable State and

Federal guidelines and regulations involving consent, protection of human subjects and donor anonymity. All brain tissues we obtained from the Brain Tissue Bank are de-identified.

Following formalin-fixed brain tissues were obtained from the Brain and Tissue Bank at UMB: COVID-19 autism (ASD, ID #6436, 38 year-old, #6437, 30 year), COVID-19 Alzheimer's disease (AD, #6535, 77 year), age-matched non-COVID-19 controls (6 cases), non-COVID-19 ASD (6 cases), non-COVID-19 FTD (frontotemporal dementia, 4 cases), and apparently healthy subjects (9 cases). We also obtained 4 cases of non-COVID-19 AD from the NIH NeuroBioBank. Samples of three brain regions were obtained from individual: dorsolateral prefrontal cortex (Broca area 8), inferior frontal cortex (Broca area 44), entorhinal cortex.

Following frozen brain tissues were also obtained from the Brain and Tissue Bank. The frozen tissues were used for RNA extraction followed by reverse transcription and PCR detection of SARS-CoV-2 with CDC specific primers. The frozen tissues include SARS-CoV-2 infected lung and brain tissues (ASD, #6436), age-matched non-COVID-19 ASD controls and FTD controls.

In addition, paraffin sections and frozen brain tissues of the subjects of COVID-19 FTD (1 case) and COVID-19 individual without underlying condition, and non-COVID-19 AD (3 cases) were obtained from the Biomarker Laboratory and Biorepository at University of Southern California Alzheimer's Therapeutic Research Institute (USC ATRI) at University of California San Diego (UCSD).

Neuronal Cells

Primary Human Neurons were obtained from Neuromics (CA3 Bioscience, MN, USA). The cells were maintained in neuron growth medium supplemented (CA3 Bioscience, MN, USA) with 10% FBS at 37 °C in a humidified atmosphere of 5% CO_2 in culture flask.

Immunohistology staining of spike protein and markers of neural cells and programmed cell death

The formalin-fixed brain tissue blocks were immersed in 30% sucrose, then embed in OCT cryostat sectioning medium. The tissues were sectioned on a cryostat at 10 μm. After rehydrated, the sections were treated with 2% H_2O_2 for 15 minutes to quench the endogenous peroxidase. The staining was performed as previously described [1,2]. Briefly, the slices were incubated with blocking solution consisting of 4% normal donkey serum (NDS), 0.2% triton (TX)-100 in phosphate-buffered saline (PBS) for 60 min, then with primary antibody diluted in blocking solution at 4 °C overnight. The slices were washed with PBS and incubated for 1 h in a biotinylated secondary antibody anti-mouse or rabbit (depending on the host species producing the primary antibodies). After three times of PBS washes, the sections were incubated in ABC solution (1:500; Vectastain Elite Kit) for 1h. The ABC solution was prepared and placed on ice for 30 minutes before use. Antibody labeling was then visualized via precipitation with a diaminobenzidine (DAB, 10mg/50ml) chromogen solution in PBS + 0.003% H_2O_2 (brown products) or with DAB in 0.175 M sodium acetate + 0.5% nickel ammonium sulfate + 0.003% H_2O_2 (for Ni-DAB staining, black products). If necessary, the sections were counterstained with hematoxylin before coverslip.

For immunohistology dual labeling, the sections were subject Ni-DAB staining with first primary antibody as described above. After PBS wash, the sections were re-blocked for 1 hours and following incubation with the second primary antibody at 4ºC overnight. Next day, the sections were washed with PBS and incubated with alkaline phosphatase (AP)-conjugated goat secondary antibody (1:200) for 1 h, followed by incubation with AP red substrate (1:100) for 20-30 minutes.

DAB-stained sections were counterstained with hematoxylin. Sections were immersed in hematoxylin solution for 3 min and rinsed in running tap water until rinse water is colorless. After

differentiation by dipping slides 10 times in acid rinse solution (1% hydrochloric acid (HCl) in 70% ethanol), the slides were incubated in the bluing solution (1.5% lithium carbonate) for 30 s. There is no hematoxylin counterstaining performed for Ni-DAB or Ni-DAB/AP dual labeling before dehydrate and coverslip.

Dehydrate and coverslip sequence: 70% ethanol, 3 minutes; 95% ethanol I and II, 3 minutes for each; 100% ethanol I and II, 3 minutes for each; xylene I and II, 5 minutes for each. Mounting medium: Permount Mounting Medium.

Aβ and p-Tau Immunohistochemistry

β-amyloid (Aβ) and phospho-tau (pTau) Immunohistochemistry was carried out as previously described [3]. Briefly, the coronal sections were rehydrated, and endogenous peroxidase was quenched by treating with 0.3% H_2O_2. For Aβ staining, the antigen retrieval was carried by using 70% formic acid for 20 minutes. Antigen retrieval for the other antibodies was by autoclaving at 120°C for 5 min. The primary antibody was applied on the sections at 4°C overnight, followed by 60-min incubation with specific secondary antibody coupled with HRP (Histofine simple stain MaxPo M/R, Nichirei Bioscience Inc., Japan) at room temperature. DAB reaction was performed to visualize the color. All antibody dilutions and washing steps were performed in phosphate buffer, pH 7.2. HRP intensities and cell counts in 3 different regions (Frontal Cortex, Entorhinal Cortex) in three sections/slices from each group were measured using the ImageJ Fiji platform. Data were represented as staining intensity per square millimeter. Because the MaxPo M/R antibodies are Fab fragments, the blocking is not necessary.

Thioflavin staining

The Aβ staining Thioflavin-T were performed following the similar antigen protocol. After blocking with 5% goat serum for 30 minutes overnight incubation with anti Aβ antibody 6E10

were performed. In the following day the brain sections were probed with Alexa-fluor594 labeled secondary antibody. After an extensive washing, Thioflavin-T (0.1% in 50% DMSO) were applied over the brain sections for 5 minutes. An extensive washing was performed using PBS containing 0.05% tween20. Furthermore, the fluorescent background was quenched with Tureblack (Biotium, USA). Thioflavin-T and Alexa-fluor594 intensity were measured using a fluorescence laser microscope (LSM780, Zeiss, Germany).

Immunofluorescent staining

For immunofluorescence staining, cells were cultured on a collagen-coated coverslip. After specific treatments, cells were fixed with 4% paraformaldehyde-PBS. The cell membrane was permeabilized with 0.25% Triton-X100 and/or 5 mg/ml digitonin followed by blocking with 5% BSA. After probing with primary antibodies, specific Alexa-fluor labeled secondary antibody were used. 4',6-Diamidino-2-phenylindole dihydrochloride (DAPI) staining was used to visualize the nuclei (Thermo Fisher Scientific). Fluorescence was assessed using a fluorescence laser microscope (LSM780, Zeiss, Germany).

Detection of SARS-CoV-2 RNA using RNAscope

RNA *In situ* hybridization in FFPE slides was performed by using the RNAScope 2.5 HD Detection (RED) Kit (ACD, CA), based on the protocol provided by the manufacturer. Briefly, after deparaffinization and antigen retrieval, the slides were hybridized with the 40-ZZ positive-sense RNA probe, V-SARS-CoV-2-S (Ref#: 854841, ACD) in the oven at 40 ºC for 2 hours. We then washed the slides with 1 X Wash Buffer for 2 min twice. The remaining hybridization procedure at 40 ºC include: 1) Amp 1, 30 min; 2) Amp 2, 15 min; 3) Amp, 30 min; 4) Amp 4, 15 min; 5) Amp 5, 30 min, and 6) Amp 6, 15 min with an interval of repeated 1X Wash buffer for 2 min. Subsequently, the signals were detected by incubating with a mixture of RED-B and RED-A

at ratio of 1:60 for 10 min at room temperature followed by counterstaining with 50% hematoxylin for 2 min.

Generation of human induced pluripotent stem cells (hiPSCs)

Human fibroblast from Coriell Institute were induced into pluripotent stem cell with CMV promoter Thomson factors lentivirus set which contains Lenti-virus harboring Oct4, Sox2, Nanog, and Lin28 (Cat#: G353, ABM Inc., Canada). Briefly, human fibroblasts were seeded on 6 well plate with 8 x 10^4 per well at day -2 and transduced with Lenti-virus particles (MOI of 4:3:3:3). Cells were cultured for 7 days and replated at 2 x 10^4 cells per well of 6 well plate on irradiated mouse embryonic fibroblasts (MEF) feeder layer. From day 8, medium was replaced with Knockout DMEM (Invitrogen) supplemented with 20% Knockout Serum Replacer (KSR, Invitrogen), 0.1 mM nonessential amino acids (Invitrogen), 2 mM GlutaMAX (Invitrogen), 0.1 mM β-mercaptoethanol (Sigma-Aldrich, St. Louis, MO), 10 ng/ml recombinant human basic fibroblast growth factor (Invitrogen) (hiPSC medium). On week 3-4, iPSCs were identified from morphology change and picked out into 48-well plates with MEF feeder.

Neuron differentiation from hiPSCs.

hiPSCs were differentiated into neurons as described with modification (Nat Med. 2018 May;24(5):647-657). hiPSCs dissociated with collagenase IV (Stem Cell Technologies) were cultured in suspension to form embryoid bodies (EB) in hES medium without bFGF for 5 days followed by maintenance in NIM medium containing Dulbecco's modified Eagle's medium/F12 and Neurobasal Medium (1:1, Thermo Fisher), 1% N2 Supplement (Life Technologies), 1% B27 Supplement (Life Technologies), nonessential amino acids, and 0.5% penicillin/streptomycin (Life Technologies) supplemented with inhibitors of the TGF-β receptor (SB431542, Stemgent; 5 μM) and the bone morphogenetic protein receptor (LDN-193189, Stemgent; 0.25 μM). On day 7,

spheres were transferred to wells coated with Matrigel (BD Biosciences) and grown in NPM medium which is same to NIM medium but replace SB431542 and LDN-193189 with 10 ng/ml bFGF (PeproTech), 10 ng/mL epidermal growth factor (EGF) (PeproTech), and 2 μg/ml heparin (Sigma). On day 15, medium was changed to NDM medium which is same to NPM medium but replace bFGF, EGF and heparin in NPM with brain-derived neurotrophic factor (10 ng/ml; PeproTech), and glial cell–derived growth factor (10 ng/ml; PeproTech). Around day 20, neurons were observed and were further differentiated for 30 days.

Immunofluorescent staining iPSCs-derived neurons

Neurons derived from AD or Control (from healthy individuals) hiPSCs with or without SARS-CoV-2 infection were fixed in 4% paraformaldehyde (PFA) for 10 minutes followed by blocking in 5% bovine serum albumin in PBST (0.1% Triton X-100 in PBS) for 10 minutes. The following antibodies were used as primary antibodies: Spike (1:200), Tuj1 (1:500), ACE2 (1:200), NRP1 (1:200), NeuN (1:200), GFAP (1:200), c-Cas3 (1:200). Normal rabbit or mouse IgG using the same dilutions as primary antibodies were used as controls. After washing with PBS, neurons were incubated with secondary antibodies. Then, neurons were counterstained with DAPI and mounted with aqueous mounting medium (Sigma, St Louis, MO). Images were captured under a microscope (Keyence BZ X700, Osaka, Japan).

SARS-CoV-2 production and infection of hiPSCs derived neurons

The stock of SARS-CoV-2 virus (CDC, WA-1 strain - BEI #NR-52281, and SARS-CoV-2 GFP generously provided by Dr. Ralph S. Baric, at the Department of Epidemiology and Department of Microbiology and Immunology, University of North Carolina at Chapel Hill), were prepared by infection of Vero E6 cells for two days when CPE (cytopathic effects) was starting to become visible. Media were collected and clarified by centrifugation prior to being aliquoted for storage

at −80 °C. Neurons derived from hiPSCs were infected with SARS-CoV-2 at 5 x 10^3, 1 x 10^4, or 2 x 10^4 plaque forming units (pfu) per well of 6 well plate for 48 h in NDM medium. All work with infectious virus was performed in a Biosafety Level 3 laboratory and approved by our Institutional Biosafety Committee.

SARS-CoV-2 Titering by semi-solid plaque assay

VeroE6 cells were plated in 12 well plates with 2x10^5 cells per well one day prior to processing. On the day of processing, samples were serially diluted 1:10 and 200uL of each sample dilution was added to each well in singlet and incubated for 1 hour at 37°C (5% CO2) with rocking every 15 minutes. Following incubation, 2 mL of a semi-solid agar overlay, DMEM (gibco) containing 4% fetal bovine sera (gibco) and 2% agarose, was added to each well. Plates are incubated for 3 days at 37°C (5% CO2) before plates were fixed with 4% paraformaldehyde, stained with crystal violet stain, and plaques counted.

Neural maturation, siRNA Transfection, and Lenti virus transduction

Primary Human Neurons obtained from Neuromics (Edina, MN) grow for four weeks in the Neuromics growth medium supplemented with brain derived neurotropic factor (BDNF). Medium were changed every 2 days. For further experiment, cells were plated on a 6-well plate in neuron growth medium supplemented with 5% FBS. siRNA transfection was carried out using X-tremeGENE siRNA transfection reagent (Roche, Basel, Switzerland) at 60% cell confluency. Medium was replaced with fresh medium 24 hours post-transfection and maintained for additional 48 hours. Lentivirus mediated overexpression of the FCGR, LILRB5 and OTOR carried out using virus particles obtained from OriGene (Rockville, MD). Virus transduction were carried out at 5.0 MOI using polybrene. GFP expressing lenti-particles were used as the control.

RNA sequencing

mRNAs were extracted from neurons derived from AD or Control hiPSCs with or without SARS-CoV-2 infection and sequenced at BGI on DNBSeq platform. Briefly, mRNAs were extracted with Trizol reagent. First-strand cDNA was generated using random hexamer-primed reverse transcription, followed by a second-strand cDNA synthesis. The synthesized cDNA was subjected to end-repair and then was 3' adenylated. Adapters were ligated to the ends of these 3' adenylated cDNA fragments, followed by PCR. PCR products were purified with Ampure XP Beads and dissolved in EB solution. Library was validated on the Agilent Technologies 2100 bioanalyzer. The double stranded PCR products were heat denatured and circularized by the splint oligo sequence. The single strand circle DNA were formatted as the final library. The library was amplified with phi29 to make DNA nanoball (DNB) which had more than 300 copies of one molecular. The DNBs were load into the patterned nanoarray and single end 50 (pair end 100) bases reads were generated in the way of sequenced by synthesis.

Quantitative reverse transcription PCR

mRNAs were extracted from neurons derived from AD or Control hiPSCs with or without SARS-CoV-2 infection in Trizol reagent (Thermofisher, Waltham, MA) and followed by cDNA synthesis with SuperScript™ III Reverse Transcriptase kit (ThermoFisher). RT-PCR were performed with PowerUp™ SYBR™ Green Master Mix (ThermoFisher) with 45 cycles and PCR products were loaded into 2% agarose gel and run at 75 v for 5.5 h. Gel Image were recorded with Bio-Rad ChemiDoc MP imaging system (Hercules, CA).

QUANTIFICATION AND STATISTICAL ANALYSIS

In the experiment assessing the impact of SARS-CoV-2 virus on the brain pathology, we analyzed (a) 5 Covid19 samples consisting of AD-Covid19 (1 case), FTD-Covid19 (1 case), ASD-Covid19

(2 cases), and Covid-19 without underlying condition (1 case); (b) 6 cases of sporadic AD as the controls; and (c) 8 cases of age-matched, non-Covid-19 healthy controls. Labeled cells from at least 3 random fields ($n \geq 3$) were counted. Data are presented as the means ± standard errors (SEs). Student's t test was used for two group comparisons. One-way ANOVA was performed for comparisons of more than two group using graphPad prism software v7. In ANOVA, a *Tukey* test was used to estimate the significance between groups. Differences were considered statistically significant when $P < 0.05$.

In the experiment with cell culture studies, we differentiated neurons from 3 iPSC lines derived from AD fibroblast cells and 3 lines from healthy subjects as the controls. The experiments were repeated in triplicate as we previously described [4,5]. Data are presented as the means ± standard errors (SEs). Student's *t* test was used for two group comparisons. One-way ANOVA plus *Tukey* test was performed for comparisons of more than two group. Differences were considered statistically significant when $P < 0.05$.

Reference:

1 Shen, W. B. *et al.* Environmental neurotoxin-induced progressive model of parkinsonism in rats. *Ann Neurol* **68**, 70-80, doi:10.1002/ana.22018 (2010).

2 Shen, W. B. *et al.* Cell-Based Therapy in TBI: Magnetic Retention of Neural Stem Cells In Vivo. *Cell Transplant* **25**, 1085-1099, doi:10.3727/096368915X689550 (2016).

3 Elahi, M. *et al.* Region-Specific Vulnerability to Oxidative Stress, Neuroinflammation, and Tau Hyperphosphorylation in Experimental Diabetes Mellitus Mice. *J Alzheimers Dis* **51**, 1209-1224, doi:10.3233/JAD-150820 (2016).

4 Xu, C. *et al.* Maternal diabetes induces senescence and neural tube defects sensitive to the senomorphic rapamycin. *Science Advances* **7**, eabf5089 (2021).

5 Wang, F. *et al.* Ask1 gene deletion blocks maternal diabetes-induced endoplasmic reticulum stress in the developing embryo by disrupting the unfolded protein response signalosome. *Diabetes* **64**, 973-988, doi:10.2337/db14-0409 (2015).

Resource Tables

Antibody	Sources	Identifier
Rabbit anti-SARS-CoV-2 spike glycoprotein antibody	Abcam	Cat# ab272504; RRID: AB_2847845
Rabbit anti-SARS Nucleocapsid Protein Antibody	Novus	Cat# NB100-56576; RRID:AB_838838
Rabbit anti-human ACE2 polyclonal antibody	Thermo Fisher Scientific	Cat# PA5-20046; RRID: AB_1115262
rabbit anti-neuropilin-1 antibody	Abcam	Cat# ab81321; RRID: AB_164073
Mouse anti-Glutamate Decarboxylase, 65 kDa Isoform (GAD65), clone GAD-6 antibody	millipore	Cat# mAB351; RRID: AB_2263126
Mouse anti-Glutamine Synthetase, clone GS-6 antibody	millipore	Cat# MAB302; RRID: AB_2110656
Rabbit anti-NeuN antibody	Abcam	Cat# ab177487; RRID: AB_2532109
Anti-Galactocerebroside antibody produced in rabbit	Sigma-Aldrich	Cat# 9152; RRID: AB_259984
Rabbit anti-Glial Fibrillary Acidic Protein (GFAP) antibody	Agilent	Cat# Z0334; RRID: AB_10013382
Anti-β-Amyloid, 1-16 Antibody (Previously Covance catalog# SIG-39300)	Biolegend	Cat# 803014; RRID:AB_2728527
β-Amyloid (D3D2N) Mouse mAb	Cell Signaling Technology	Cat# 15126; RRID:AB_2798720
Rabbit anti-phospho-Tau (Ser202, Thr205) Monoclonal Antibody (AT8)	Thermo Fisher Scientific	Cat# MN1020; RRID: AB_223647
Anti-β-Amyloid (D54D2) XP® Rabbit mAb antibody	Cell Signaling Technology	Cat# 8243; RRID: AB_2797642
Neurofilament-L (C28E10) Rabbit mAb antibody	Cell Signaling Technology	Cat# 2837; RRID: AB_823575
Rabbit anti-Cleaved Caspase-3 (Asp175) Antibody	Cell Signaling Technology	Cat# 9661; RRID: AB_2341188
Neuronal Class III beta-Tubulin (TUJ1) Mouse Monoclonal Antibody, Purified	Covance	Cat# MMS-435P; RRID: AB_231377
Rabbit anti Iba1, Rabbit antibody	FUJIFILM Wako	Cat# 019-19741; RRID:AB_839504
Rabbit anti-RIP3 (phospho S227) antibody [EPR9627]	Abcam	Cat# ab209384; RRID: AB_2714035
Rabbit anti-MLKL (phospho S358) antibody	Abcam	Cat# ab187091; RRID: AB_2619685
Mouse anti-TRANSFERRIN RECEPTOR Monoclonal Antibody (H68.4)	Thermo Fisher Scientific	Cat# 13-6800; RRID: AB_86623

Rabbit anti-FACL4 (ASCL4) antibody [EPR8640]	Abcam	Cat# ab155282; RRID: AB_2714020
Rabbit anti-DPP4/CD26 (D6D8K) antibody	Cell Signaling Tech	Cat# 67138; RRID: AB_2728750
Rabbit anti-phospho-Tau (Ser396) Polyclonal Antibody	Thermo Fisher Scientific	Cat# 44-752G; RRID: AB_253374
Rabbit anti-phospho-Tau (Ser214) Polyclonal Antibody	Thermo Fisher Scientific	Cat# 44-742G; RRID: AB_2533740
Rabbit anti-pTau-Ser202(PS202) antibody	In house	
Rabbit Anti-Amyloid oligomer, abeta, oligomeric antibody	Millipore	Cat# AB9234; RRID: AB_570955
Human IL-1 beta/IL-1F2 MAb (Clone 8516) antibody	R and D System	Cat# MAB201; RRID:AB_358006
Mouse Anti-Human IL-6 Monoclonal antibody, Unconjugated, Clone 1936	R and D System	Cat# MAB2061; RRID: AB_2127616
CD3 Monoclonal Antibody (OKT3), Functional Grade	Thermo Fisher Scientific	Cat# 16-0037-81; RRID: AB_468854
Mouse anti-human CD20 antibody	Biolegend	Cat# 302301; RRID:AB_314249
F8/40 mouse monoclonal antibody	Santa Cru Biotech	Cat# sc377009
Biotin-conjugated Goat anti-mouse IgG	Vector Lab	Cat# BA-9200; RRID:AB_2336171
Biotin-conjugated Goat anti-Rabbit IgG	Vector Lab	Cat# BA-1000; RRID:AB_2313606
Alexa488-donkey anti-mouse IgG	Invitrogen	Cat# A21201; RRID:AB_141630
Alexa488-donkey anti-rabbit IgG	Invitrogen	Cat# A21206; RRID:AB_2535792
Alexa594-donkey anti-mouse IgG	Invitrogen	Cat# A21203; RRID:AB_141633
Alexa594-doneky anti-rabbit IgG	Invitrogen	Cat# A21207; RRID:AB_141637
Goat anti-mouse IgG, alkaline phosphatase conjugated	thermo Fisher Scientific	Cat# A21060; RRID:AB_2536528
Goat anti-rabbbit IgG, alkaline phosphatase conjugated	thermo Fisher Scientific	Cat# A16099; RRID: AB_2534773
Histofine Simple Stain MAX PO (R)	Nichirei Bioscience	Cat# 414141F
Histofine Simple Stain MAX PO (M)	Nichirei Bioscience	Cat# 414131F

Viral strain	Sources	Identifier
SARS-CoV-2, WA-1 strain - BEI	CDC	Cat #NR-52281
SARS-CoV-2 GFP	provided by Dr. Ralph S. Baric	Hou et al.
CMV Promoter Thomson Factors Lentivirus Set	ABMgood, Canada	Cat# G353

Reagent or Resources	Sources	Identifier
Normal Donkey Serum	Sigma	Cat# D9663
PBS, pH7.4	Quality Biological	Cat# 119-069-131
Triton X100	Sigma	Cat# X100
Hydrogen peroxide (H2O2)	Sigma	Cat# H1009
Antigen Retriever, Citrate buffer, pH6	Sigma	Cat# C9999
Antigen Retriever, formic acid	Sigma	Cat# F0507
VECTASTAIN Elite Kits	VectorLab	Cat# PK-6100
SignalStain® Vibrant Red AP Substrate Kit	Cell Signal Tech	Cat# 76713
DAB (3,3′-Diaminobenzidine tetrahydrochloride hydrate)	Sigma	Cat# D5637
Hematoxylin Solution, Harris Modified	Sigma	Cat# HHS32
Tissue-Plus OCT Compound	Fisher Scientific	Cat# 23-730-571
Ammonium Nickel (II) sulfate hexahydrate	Sigma	Cat# A1827
Lithium Carbonate	Sigma	Cat# 255823
Ethanol, Decon Labs, 200 proof	VWR	Cat# 71002-426
Xylenes Histological Grade	Sigma	Cat# 534056
Thioflavin-T	Sigma	Cat# T3516
DAPI (4',6-diamidino-2-phenylindole)	Thermo Fisher Scientific	Cat# D9542
Permount mounting medium	Fisher	Cat# SP15100
Fluorescence mounting medium	Sigma	Cat# F4680
Paraformaldehyde (4%, pH7.4) in PBS	Thermo Fisher Scientific	Cat# J61889
RNAscope® 2.5 HD Reagent Kit-RED	ACD	Cat# 322350
RNAscope® Probe	ACD	Cat# 854841
Knockout DMEM medium	Thermo Fisher Scientific	Cat# 10829018
Knockout serum replacer	Thermo Fisher Scientific	Cat# 10828028
Nonessential amino acids	Thermo Fisher Scientific	Cat# 11140050
GlutaMAX	Thermo Fisher Scientific	Cat# 35050061
β-mercaptoethanol	Sigma	Cat# M3148
Recombinant human basic fibroblast growth factor	Thermo Fisher Scientific	Cat# 13256-029
Collagenase IV	Stem Cell Technologies	Cat# 17104019
DMEM/F12	Thermo Fisher Scientific	Cat# 11320033
N2 supplement	Thermo Fisher Scientific	Cat# 17502048
Neurobasal medium	Thermo Fisher Scientific	Cat# 21103049

B27 supplement	Thermo Fisher Scientific	Cat 17504044
Penicillin/streptomycin	Thermo Fisher Scientific	Cat# 15140122
Stemolecule SB431542, TGF-β inhibitor	Reprocell	Cat# 04-0010-10
LDN-193189, inhibitor of bone morphogenetic protein receptor	Reprocell	Cat# 04-0074
Matrigel	BD Biosciences	Cat# 354277
bFGF	Pepro Tech	Cat# 100-18b
EGF, epidermal growth factor	Pepro Tech	Cat# 100-47
Heparin	Sigma	Cat# H4784
Brain-derived neurotrophic factor, BDNF	Pepro Tech	Cat# 450-02
Glial cell–derived neurotrophic factor, GDNF	Pepro Tech	Cat# 450-10
X-tremeGENE siRNA transfection reagent, Roche	Sigma	Cat# 6366236001
SuperScript™ III Reverse Transcriptase kit	Thermo Fisher Scientific	Cat# 18080051
PowerUp™ SYBR™ Green Master Mix	Thermo Fisher Scientific	Cat# A25742

Brain Tissue	Source	Identifier
Alzheimer's Disease (AD)-Covid19 brain tissue, Male,	NIH NeuroBioBank	UMBN #6435
Autism-Covid19 brain tissue, Female, 38 yr	NIH NeuroBioBank	UMBN #6436
Autism-Covid19 brain tissue, Male, 30 yr	NIH NeuroBioBank	UMBN #6437
Frontotemporal Dementia (FTD)-Covid19, Female, 71 yr	UCSD,	#5922
Covid19, Male, 77 yr	UCSD,	#5932
Sporadic AD, Female, 65 yr	NIH NeuroBioBank	#116311
Sporadic AD, Male, 63 yr	NIH NeuroBioBank	#116319
Sporadic AD, Male, 63 yr	NIH NeuroBioBank	#116317
Sporadic AD, Male, 79 yr	UCSD,	#5877
Sporadic AD, Female, 71 yr	UCSD,	#5875
Sporadic AD, Male, 76 yr	UCSD,	#5872
Unaffected Control, Male, 29 yr	NIH NeuroBioBank	UMBN #1502
Unaffected Control, Male, 30 yr	NIH NeuroBioBank	UMBN #6099
Unaffected Control, Female, 38 yr	NIH NeuroBioBank	UMBN #1648
Unaffected Control, Male, 38 yr	NIH NeuroBioBank	UMBN #5249
Unaffected Control, Male, 38 yr	NIH NeuroBioBank	UMBN #4592
Unaffected Control, Female, 77 yr	NIH NeuroBioBank	UMBN #1569
Unaffected Control, Male, 75 yr	NIH NeuroBioBank	UMBN #5830
Unaffected Control, female, 76 yr	NIH NeuroBioBank	UMBN #5219
ASD-Autism, 37 yr	NIH NeuroBioBank	UMBN #5027
ASD-Autism suspended, Epilepsy, 28 yr	NIH NeuroBioBank	UMBN #5934
ASD-Autism, Epilepsy, 29 yr	NIH NeuroBioBank	UMBN #5940
ASD-Austim suspended, 35 yr	NIH NeuroBioBank	UMBN #6092
ASD-Autism suspended, 36 yr	NIH NeuroBioBank	UMBN #6212
ASD-Autism suspended, 30 yr	NIH NeuroBioBank	UMBN #6381
Frontotemporal dementia, 70yr	NIH NeuroBioBank	UMBN #6220
Frontotemporal dementia, 65yr	NIH NeuroBioBank	UMBN #6019
Frontotemporal dementia, 76yr	NIH NeuroBioBank	UMBN #6264
Frontotemporal dementia, 73yr	NIH NeuroBioBank	UMBN #6207

Cell lines	Source	Identifier
iPSCs, from Familial AD, female, 31 yr	Coriell Institute	Cat# AG25367
iPSCs, from Sporadic AD, male, 60 yr	Coriell Institute	Cat# AG07376
iPSCs, from Sporadic AD, male, 83 yr	Coriell Institute	Cat# GM24666
iPSCs, from apparently healthy male, 55 yr	Coriell Institute	Cat# GM23248
iPSCs, from apparently healthy female, 36 yr	Coriell Institute	Cat# GM23279
iPSCs, from apparently healthy female, 36 yr	Coriell Institute	Cat# GM23280
Primary human neuron	Neuromics	HNC001
Vero E6 cells	ATCC	CRL-1586
mouse embryonic fibroblasts (MEF)	Thermo Fisher Scientific	Cat# A34180

Plasmid DNAs	**Source**	**Identifier**
CRYAA2_pcDNA3.1+/C-(K)-DYK	Genscript	Cat# OHu53183D
GJA8_pcDNA3.1+/C-(K)-DYK	Genscript	Cat# OHu22749D
OTOR(NM_020157.4) ORF Clone	Genscript	Cat# OHu00520D
Human LILRB5(NM_001081442.2) ORF Clone	Genscript	Cat# OHu64562D
FCGR3A(NM_000569.6) ORF Clone	Genscript	Cat# OHu27381D
PSG6(NM_001031850.4) ORF Clone	Genscript	Cat# OHu56074D

siRNAs	**Source**	**Identifier**
GJA8 siRNA	Ambion	Cat# S5769
CRYAA2 siRNA	Ambion	Cat# 3540
PSG6 siRNA	Ambion	Cat# 11312

Lentiviru	**Source**	**Identifier**
Otoraplin (OTOR) (NM_020157) Human Tagged ORF Clone	Origene	Cat# RC210984L4V
LILRB5 (NM_001081443) Human Tagged ORF	Origene	Cat# RC219303L4V
CD16 (FCGR3A) (NM_000569) Human Tagged ORF	Origene	Cat# RC206429L2V

Software and Algorithems	Source	Identifier
GraphPad Prism 7	GraphPad	NA
photoshop CS3	Adobe	NA

QPCR primers	Sources	Identifier
FCGR3A qPCR, mRNA forward: 5'-CCTCCTGTCTAGTCGGTTTGG; reverse: 5'-TCGAGCACCCTGTACCATTGA	Genbank Accession NM_000569	PrimerBank ID 24429586a1
LILRA3 qPCR, mRNA forward: 5'-AGGAGTGGGGACGTGACTT; reverse: 5'-GGTCTGGCACGGATCTGTC	Genbank Accession NM_006865	PrimerBank ID 289547630c1
TLR8 qPCR, mRNA forward: 5'-AACTGCCAAGCTCCCTACG; reverse: 5'-CAAGGCACGCATGGAAATGG	Genbank Accession NM_138636	PrimerBank ID 257196253c3
LILRB5 qPCR, mRNA forward: 5'-GACTGATCCCTGACATACCCG; reverse: 5'-GTGTCTATCTGATGCCATGACTG	Genbank Accession NM_006840	PrimerBank ID 125987589c2
OTOR qPCR, mRNA forward: 5'-TCTGGCTAGTGCTCAAGAAGA; reverse: 5'-TAACCCACGACTCCCATCTCG	Genbank Accession NM_020157	PrimerBank ID 21618345c1
TMEM140 qPCR, mRNA forward: 5'-TCGGCTTCTATAACTTCTGCCT; reverse: 5'-CTGTTGCACTGGGCTAGGAG	Genbank Accession NM_018295	PrimerBank ID 256355110c2
SIGLEC1 qPCR, mRNA forward: 5'-ATGGGGTACGCCTCCAAAC; reverse: 5'-GTGCCTCATTGGGTGTGTTG	Genbank Accession NM_023068	PrimerBank ID 89142743c1
CCL4 qPCR, mRNA forward: 5'-CTGTGCTGATCCCAGTGAATC; reverse: 5'-TCAGTTCAGTTCCAGGTCATACA	Genbank Accession NM_002984	PrimerBank ID 4506845a1
SLCO2B1 qPCR, mRNA forward: 5'-TATGTGGACATTAACCAGATGCC; reverse: 5'-CTGTGACTGCTAAGACCTTTCG	Genbank Accession NM_001145211	PrimerBank ID 312176373c2
TM4SF4 qPCR, mRNA forward: 5'-CTGTGGTTGGATTCTTGGGAG; reverse: 5'-GGGTAGCCCCATGTACTATTGG	Genbank Accession NM_004617	PrimerBank ID 325974483c2
XAF1 qPCR, mRNA forward: 5'-GCTCCACGAGTCCTACTGTG; reverse: 5'-GTTCACTGCGACAGACATCTC	Genbank Accession NM_017523	PrimerBank ID 378925606c1
KCNQ5 qPCR, mRNA forward: 5'-TGTTGTCGATATAGAGGATGGCA; reverse: 5'-GAGTGCAGACGTGGCAAAAAT	Genbank Accession NM_001160134	PrimerBank ID 236462241c3
ANGPTL1 qPCR, mRNA forward: 5'-AGAAAGGAAAGCCGTAACATGAA; reverse: 5'-TCCCTGTATCTTGTTGCCATCT	Genbank Accession NM_004673	PrimerBank ID 38327520c3
COL21A1 qPCR, mRNA forward: 5'-GGCCACAAATAGCAGTTACCT; reverse: 5'-AGCCTTCATCAAACAACGTCTTA	Genbank Accession NM_030820	PrimerBank ID 90577174c2
KLHDC7B qPCR, mRNA forward: 5'-GCACCATGCACAACTACCTGT; reverse: 5'-ATTCGCCACCGATGGCATAG	Genbank Accession NM_138433	PrimerBank ID 206597555c1
HAND2 qPCR, mRNA forward: 5'-CGCCGACACCAAACTCTCC; reverse: 5'-TCGCCATTCTGGTCGTCCT	Genbank Accession NM_021973	PrimerBank ID 88999597c2
COMP qPCR, mRNA forward: 5'-CGAGTCCGCTGTATCAACACC; reverse: 5'-TCCGTGCAAACCTGCTTGT	Genbank Accession NM_000095	PrimerBank ID 40217842c2
SLC22A4 qPCR, mRNA forward: 5'-TGGTAGCCTTCATACTAGGAACA; reverse: 5'-TGGCAGCAGCATATAGCCAAC	Genbank Accession NM_003059	PrimerBank ID 24497489c1
PTPRH qPCR, mRNA forward: 5'-TCGCCCTATGCTGGGAAGT; reverse: 5'-TCTGCCCATACAGAGAATGTGT	Genbank Accession NM_002842	PrimerBank ID 241896923c2
FGF10 qPCR, mRNA forward: 5'-CATGTGCGGAGCTACAATCAC; reverse: 5'-CAGGATGCTGTACGGGCAG	Genbank Accession NM_004465	PrimerBank ID 4758359c1
VIT qPCR, mRNA forward: 5'-TGTGCTTGATAATTCAGGAGGGA; reverse: 5'-GATTGGACACCGTTGGAATAACT	Genbank Accession NM_001177970	PrimerBank ID 295789106c2
GJA8 qPCR, mRNA forward: 5'-GACCCTGCTGAGGACCTACAT; reverse: 5'-CCCAACTCCATCACGTTGAG	Genbank Accession NM_005267	PrimerBank ID 281182631c2

PSG6 qPCR, mRNA forward: 5'-AAGCTGCCCATGCCTTACATC; reverse: 5'-AGGTGTAGTTCCGACTCTTAGG	Genbank Accession NM_001031850	PrimerBank ID 141802170c1
Amyloid precursor protein (APP), mRNA, forward: 5'-GTCTCTCTCCCTGCTCTACAA; reverse: 5'-GGCCAAGACGTCATCTGAATAG	Genbank Accession NM_000484	Cairns et al., 2020
ABeta secretase 1 (BACE1), mRNA, forward: 5'-CCATCCTTCCGCAGCAATA; reverse: 5'-CGTAGAAGCCCTCCATGATAAC	Genbank Accession NM_012104	Cairns et al., 2020
Tumor necrosis factor alpha (TNFα), mRNA, forward: 5'-GAGGCCAAGCCCTGGTATG; reverse: 5'-CGGGCCGATTGATCTCAGC	Genbank Accession NM_000594.4	Cairns et al., 2021
Presenilin 1 (PSEN1), mRNA, forward: 5'-TGGCTACCATTAAGTCAGTCAGC; reverse: 5'-CCCACAGTCTCGGTATCTTCT	Genbank Accession NM_000021	Cairns et al., 2024
Presenilin 2 (PSEN2), mRNA, forward: 5'-CTGACCGCTATGTCTGTAGTGG; reverse: 5'-CTTCGCTCCGTATTTGAGGGT	Genbank Accession NM_012486	Cairns et al., 2025
Interleukin 6 (IL-6), mRNA, forward: 5'-TCAATATTAGAGTCTCAACCCCC; reverse: 5'-TTGTTTTCTGCCAGTGCCTC	Genbank Accession NM_012486	Cairns et al., 2026
Interleukin 1beta (IL-1β), mRNA, forward: 5'-CAGAAGTACCTGAGCTCGCC; reverse: 5'-AGATTCGTAGCTGGATGCCG	Genbank Accession NM_000576.2	Cairns et al., 2027
Interferon gamma (INFγ), mRNA, forward: 5'-ACTGTCGCCAGCAGCTAAAA; reverse: 5'-TATTGCAGGCAGGACAACCA	Genbank Accession NM_000619	Cairns et al., 2028
Glyceraldehyde 3-phosphate dehydrogenase (GAPDH), mRNA, forward: 5'-ATTGCCCTCAACGACCACT; reverse: 5'-ATGAGGTCCACCACCCTGT	Genbank Accession NM_002046.5	Cairns et al., 2030
CDC 2019-nCoV_N1, forward: 5'-GAC CCC AAA ATC AGC GAA AT	CDC	IDT, Cat# 10006821
CDC 2019-nCoV_N1, reverse: 5'-TCT GGT TAC TGC CAG TTG AAT CTG	CDC	IDT, Cat# 10006822
2019-nCoV_N_Positive Control	IDT	IDT, Cat# 10006625